nutrients

MDPI

Article

Liubao Tea Extract Attenuates High-Fat Diet and Streptozotocin-Induced Type 2 Diabetes in Mice by Remodeling Hepatic Metabolism and Gut Microbiota

Jichu Luo [1,†], Zhijuan Wei [1,†], Yuru Tan [1], Ying Tong [1], Bao Yang [2], Mingsen Wen [1], Xuan Guan [1], Pingchuan Zhu [4], Song Xu [1], Xueting Lin [1], Qisong Zhang [1,2,3,*]

[1] Guangxi Key Laboratory of Special Biomedicine, School of Medicine, Guangxi University, Nanning 530004, China; luojichu1999@163.com (J.L.); weizhijuan2022@163.com (Z.W.); 15894549320@163.com (Y.T.); tongying0206@163.com (Y.T.); q954637097@163.com (M.W.); guanxuan010203@163.com (X.G.); fighting68_xusong@163.com (S.X.); kyl05170606@163.com (X.L.)
[2] Hubei Provincial Key Laboratory of Occurrence and Intervention of Rheumatic Diseases, Hubei Minzu University, Enshi 445000, Hubei, China; ybsept@hbmzu.edu.cn (B.Y.)
[3] Center for Instrumental Analysis, Guangxi University, Nanning 530004, China
[4] State Key Laboratory for Conservation and Utilization of Subtropical Agro-Bioresources, Guangxi University, Nanning 530004, China; zhupingchuan12@163.com (P.Z.)
* Correspondence: zhangqisong@gxu.edu.cn (Q.Z.); Tel.: +86-0771-3387105 (Q.Z.)
† These authors contributed equally to this work.

Abstract: Background: Type 2 diabetes (T2D) has become a serious global public health concern. Liubao tea (LBT) has demonstrated beneficial effects on gut microbiota and glucose-lipid metabolism, holding promising therapeutic potential for T2D, however, its underlying mechanisms remain unclear. This study aims to elucidate the potential mechanisms of Liubao tea extract (LBTE) against T2D. **Methods**: LC-MS technology was used to identify the chemical components of LBTE, and combined with network pharmacology and molecular docking to screen its potential active ingredients and targets for improving T2D. Therapeutic efficacy was assessed in high-fat diet/streptozotocin (HFD/STZ)-induced diabetic mice via serum biochemical analyses, histopathological examinations. Serum metabolomics, 16S rRNA sequencing, quantification of short-chain fatty acids (SCFAs), quantitative real-time PCR (qPCR), and antibiotic-treated pseudo-germ-free models were employed to elucidate the underlying mechanisms. **Results**: LBTE effectively reduced blood glucose levels and improved lipid metabolism, primarily by promoting hepatic glycogen synthesis and suppressing glycerophospholipid synthesis. LBTE also alleviated hepatic inflammation by modulating inflammatory cytokine expression. Additionally, LBTE reshaped the gut microbiota profiles by decreasing harmful bacteria and increasing SCFA-producing bacteria, resulting in elevated fecal SCFAs. SCFAs contributed to improving hepatic metabolism and inflammation, enhancing intestinal barrier function. Notably, these effects were abolished by antibiotic-induced microbiota depletion, confirming the microbiota-dependent mechanism of LBTE. Quercetin, luteolin, genistein, and kaempferol were considered as potential active ingredients contributing to the antidiabetic effects of LBTE. **Conclusions**: These findings provide novel perspectives on the viability of LBTE as a complementary strategy for T2D prevention and management.

Keywords: Type 2 diabetes; Liubao tea extract; Hepatic metabolism; Gut microbiota; Short-chain fatty acids

Academic Editor: Firstname Lastname

Received: date
Revised: date
Accepted: date
Published: date

Citation: To be added by editorial staff during production.

Copyright: © 2025 by the authors. Submitted for possible open access publication under the terms and conditions of the Creative Commons Attribution (CC BY) license (https://creativecommons.org/licenses/by/4.0/).

1. Introduction

Diabetes has become a critical global health concern [1], with projections estimating that the global diabetic population will reach 783.2 million by 2045, of which approximately 90% are expected to be type 2 diabetes (T2D) cases [2]. T2D is a severe and complex metabolic disorder characterized by insulin resistance and impaired insulin secretion, leading to chronic hyperglycemia and disrupted glycometabolism. Current therapeutic strategies predominantly rely on pharmacological interventions, which often require lifelong administration and are associated with adverse effects, including gastrointestinal disturbances and potential hepatorenal toxicity [3]. Therefore, the development of safer and more effective alternatives for T2D management remains an urgent priority.

Tea (*Camellia sinensis* (L.) Kuntze) has a long history of medicinal use in China, traditionally attributed to the legend of Shen-Nong tasting herbs. Its therapeutic applications have evolved over thousands of years and are well documented in classical medical texts and traditional Chinese pharmacopeias [4,5]. Among the various tea types, dark tea, a post-fermented tea characterized by its unique organoleptic attributes, has been traditionally used in medicinal formulations for the prevention and treatment of obesity and diabetes [6]. Liubao tea (LBT), a representative Chinese dark tea with a history of over 1,500 years, is a nationally recognized geographical indication product originating from Wuzhou, Guangxi [7,8]. Modern pharmacological studies have revealed that LBT is rich in polysaccharides, polyphenols, and flavonoids, exhibiting hypolipidemic, hepatoprotective, and hypoglycemic bioactivities [9]. Our previous studies also found that LBT ameliorated non-alcoholic fatty liver disease (NAFLD) and hyperlipidemia by modulating lipid metabolism and gut microbiota [10,11]. Although preliminary evidence indicates that LBT may alleviate T2D symptoms [12,13], its bioactive constituents and underlying mechanisms remain largely unclear.

The gut microbiota, a complex and dynamic ecosystem, plays a crucial role in host metabolic homeostasis. Gut microbiota-derived metabolites, such as short-chain fatty acids (SCFAs), influence glucose and lipid metabolism by interacting with G-protein-coupled receptors (GPCRs) and activating hepatic signaling pathways [14]. Since the introduction of the microbiome into the biomedical field, the host metabolism mediated by gut microbiota has become an important area of research, playing an important role in the pathogenesis and treatment of metabolic diseases such as diabetes [15]. (-)-Epicatechin has been found to modulate the gut microbiota and liver insulin signaling pathways to alleviate T2D [16]. Similarly, *L. gasseri CKCC1913* may exert antidiabetic effects by increasing the abundance of beneficial bacteria that produce SCFAs, some of which can reach the liver and contribute to glucose and lipid homeostasis [17]. These findings underscore the critical role of the gut microbiota and its mediated metabolism in T2D treatment. However, whether LBT can effectively improve T2D by modulating the gut microbiota and hepatic metabolism has not yet been reported, and its underlying mechanisms remain largely unexplored.

Given the complexity of metabolic disease pathogenesis, the integration of bioinformatics and multiomics has emerged as a powerful strategy to elucidate drug mechanisms and disease pathogenesis [10]. Bioinformatics serves as an important computational tool for analyzing gene expression data and identifying molecular targets and mechanisms involved in various diseases [18]. Multiomics analysis, such as metabolomics and gut microbiota profiling, offers comprehensive approaches for identifying natural product targets and elucidating their pharmacological mechanisms from multiple perspectives [19]. In particular, network pharmacology and molecular docking have been widely used to predict the bioactive components of natural products, potential targets of action, and the mechanisms of their interactions [20]. Integration with metabolomics enables more accurate identification of key metabolites and metabolic pathways associated with disease

modulation [21]. Additionally, alterations in gut microbiota composition have been shown to significantly influence host metabolic profiles and metabolic pathways [22]. Thus, the integration of bioinformatics with multiomics holds significant promise for deepening our understanding of the mechanisms by which LBT exerts its therapeutic effects in T2D.

This study aims to elucidate the underlying mechanisms by which Liubao tea extract (LBTE) exerts its antidiabetic effects, with a particular focus on the modulation of gut microbiota and microbiota-mediated metabolic pathways. The chemical composition of LBTE was preliminarily characterized through LC–MS analysis. Based on the identified constituents, network pharmacology and molecular docking analyses were employed to predict the active components, therapeutic targets, and key signaling pathways involved in its antidiabetic activity. Selected active compounds were subsequently validated using chemical standards. To assess the therapeutic efficacy of LBTE, a T2D mouse model was established through high-fat diet/streptozotocin (HFD/STZ) induction. Then, the effects of LBTE treatment were evaluated by serum biochemical analyses and histopathological examination of major tissues. Untargeted metabolomics was conducted to identify key metabolic alterations following LBTE intervention. Meanwhile, 16S rRNA gene sequencing was used to profile the gut microbiota composition and identify key genera modulated by LBTE. To further explore the underlying mechanisms, quantitative real-time PCR (qPCR) was conducted to assess the expression of genes involved in metabolic and inflammatory pathways. Additionally, pseudo-germ-free mouse models were utilized to validate the microbiota-dependent effects of LBTE. Collectively, this study is expected to provide novel insights into anti-diabetes mechanisms of LBTE and support its potential as a promising complementary strategy for the prevention and management of T2D.

2. Materials and Methods

2.1. Chemicals and reagents

MS-grade methanol, water, acetonitrile, and formic acid were purchased from Merck & Co. (Billerica, MA, USA). LBT was provided by China Tea Co., Ltd. (Wuzhou, Guangxi, China) (Batch number: S002/2022), conforming to GB/T 32719.4-2016 (Brick LPT, Second class). Standards of quercetin (C15H10O7, HPLC > 99%), luteolin (C15H10O6, HPLC > 99%), genistein (C15H10O5, HPLC > 99%), caffeine (C8H10N4O2, HPLC > 99%), naringenin (C15H12O5, HPLC > 99%) and kaempferol (C15H10O6, HPLC > 99%) were sourced from Chengdu RefMedic Biotech Co., Ltd. (Chengdu, China). Streptozotocin (STZ), metformin hydrochloride, and citrate buffer were obtained from Macklin Co., Ltd. (Shanghai, China). All other chemicals were analytical grade or higher.

2.2. Preparation and preliminary chemometric analysis of LBTE

LBTE was prepared using a modified version of a previously reported method [23], with detailed procedures provided in the Supplementary Material. In accordance with national analytical standards, major components including total polyphenols (GB/T 8313-2018), total flavonoids (SN/T 4592-2016), total free amino acids (GB/T 8314-2013), and total polysaccharides (NY/T 1676-2008), were quantified using validated chemometric protocols. The total soluble sugar content was determined using the anthrone–sulfuric acid colorimetric method, with glucose as the calibration standard.

2.3. Characterization of the chemical composition of LBTE

LBTE (1.5 mg) was dissolved in 1.5 mL of methanol and subsequently filtered through a microporous membrane (0.22 μm) to prepare the test solution. The prepared solution was analyzed and characterized using a Waters ACQUITY UPLC I-Class PLUS

System (Waters, Milford, MA) (SN: L22BSP766G) coupled with a SELECT SERIES Cyclic IMS (Milford, MA, USA) (SN: GBC086). Detailed LC-MS analytical parameters are presented in Tables S1 and S2.

2.4. Network pharmacology analysis

2.4.1. Drug target prediction and disease target identification

Active ingredients in LBTE were screened using the SwissADME database. Potential targets of the active ingredients were predicted using the SwissTargetPrediction database. T2D-related potential targets were obtained by collecting and de-duplicating data from the OMIM and GeneCards databases. The overlapping targets between the active ingredients and T2D were identified and visualized using a Venn diagram. Protein-protein interaction (PPI) analysis was performed using the STRING database and visualized in Cytoscape 3.9.1. Gene Ontology (GO) and Kyoto Encyclopedia of Genes and Genomes (KEGG) enrichment analyses were performed using the Metascape platform. The top 10 GO terms and top 20 KEGG pathways were visualized using the Wei Sheng Xin cloud platform.

2.4.2. Molecular docking

The 2D structures of the core compounds were sourced from the PubChem database and energy-minimized using the Molecular Operating Environment (MOE). The crystal structures of key proteins were retrieved from the RCSB PDB database, including AKT1 (PDB ID: 1UNQ; resolution: 0.98 Å), TNF (PDB ID: 5UUI; resolution: 1.40 Å), and GSK3B (PDB ID: 1O6L; resolution: 1.60 Å). Detailed information regarding the molecular docking procedures is provided in the Supplementary Material.

2.5. Identification of potential active ingredients in LBTE

Standards of four ingredients (quercetin, luteolin, genistein, and kaempferol) were analyzed using the same LC–MS conditions as those applied for the chemical profiling of LBTE. Each component was verified based on retention time and fragmentation information. Detailed LC-MS analytical parameters are provided in Tables S1 and S2.

2.6. Quantitative analysis of potential ingredients in LBTE

LBTE (1.5 mg) was dissolved in 1.5 mL of methanol and subsequently filtered through a microporous membrane (0.22 μm) to prepare the test solution. The sample was analyzed using an Agilent 1260 Infinity LC system (SN: DEAEQ48900) and an Agilent 6545 Q-TOF mass spectrometer (SN: SG22202E101), equipped with an ESI source (Santa Clara, CA, USA). The analytical conditions of the LC and MS equipment are provided in Tables S3 and S4. Standards of six ingredients were analyzed using instrumental methods consistent with those used for analysis of LBTE. Each compound was quantified based on retention time and exact m/z values using external calibration curves derived from chemical standards.

2.7. Experimental verification

2.7.1. Animal model and treatment

Six-week-old male Kunming (KM) mice (18-22 g) were purchased from SPF (Beijing) Biotechnology Co., Ltd. (license No.110324230101502642). Mice were randomly divided into groups according to the RAND function in Microsoft Excel. The individual mouse was considered the experimental unit within the studies. All experimental mice were housed with free access to food and water under the controlled conditions of 25 ± 2 °C temperature, 50 ± 5% relative humidity, and a 12 h light/dark cycle.

A previously reported protocol for T2D induction was followed with minor modifications [24,25]. The design of Experiment 1 is illustrated in Figure S1. After one week of acclimatization, thirty male mice were randomly assigned to five groups (n = 6 per group): normal control (NC) group, model control (MC) group, positive control (PC) group, LBTE low-dose (LBTE-L) group, and LBTE high-dose (LBTE-H) group. Except for the NC group (normal-chow diet), all mice from other groups were fed a high-fat diet (HFD) for four weeks, followed by two intraperitoneal injections of STZ (50 mg/kg), and the NC group received equivalent volumes of citrate buffer. Three days after the final injection, mice with fasting blood glucose (FBG) ≥ 11.1 mmol/L were classified as T2D mice [26]. Subsequently, mice in the LBTE-L and LBTE-H groups were orally administered LBTE at doses of 200 and 400 mg/kg, respectively, once daily for three weeks, based on previous studies with minor modifications [11,27,28]. The PC group received metformin (200 mg/kg), while the NC and MC groups received an equivalent volume of normal saline.

To investigate the microbiota-dependent effects of LBTE, a second animal experiment (Experiment 2) was conducted based on a previously described antibiotic depletion protocol with minor modifications [29]. The experimental design is depicted in Figure S2. Briefly, eighteen T2D mice were randomly assigned to three groups (n = 6 per group): MC group, MC + Antibiotic mixture (MA) group, and LBTE + Antibiotic mixture (LBTEA) group. The mice in the MA and LBTEA groups were orally administered a mixture of antibiotics (ampicillin 130 mg/kg; metronidazole 150 mg/kg; neomycin 100 mg/kg; and vancomycin 130 mg/kg) daily, and mice in the MC group were orally equivalent volume of sterile water. Additionally, mice in the LBTEA group were treated with LBTE (400 mg/kg), whereas the other groups received an equal volume of normal saline. FBG levels, body weight, food intake, and water intake were monitored weekly during the treatment period.

2.7.2. Sample collection

At the end of the experiment, all mice were euthanized, and blood samples were collected immediately. Serum was isolated by centrifugation at 5,000 rpm for 8 minutes at 4 °C and subsequently stored at − 80 °C for further analysis. Major organs and tissues were carefully excised, rinsed in cold saline, blotted dry, and weighed before being stored or processed for histological analysis.

2.7.3. Biochemical index determination

Serum levels of alanine aminotransferase (ALT), aspartate transaminase (AST), total bile acid (TBA), creatinine (Cr), uric acid (UA), total cholesterol (TC), triglycerides (TG), low-density lipoprotein cholesterol (LDL-C) and high-density lipoprotein cholesterol (HDL-C) were measured using commercial kits from Nanjing Jiancheng Bioengineering Institute (Nanjing, China), according to the manufacturer's instructions.

2.7.4. Histopathological analysis

Tissue samples from the liver, adipose tissue, heart, lung, kidney, and colon were fixed in 4% paraformaldehyde, dehydrated, washed, embedded in paraffin, sectioned (4 μm), and baked. Hematoxylin and eosin (H&E) staining was performed on all tissue sections, while liver sections were additionally stained with Oil Red O to evaluate lipid accumulation. Histopathological changes were observed under a light microscope.

2.8. Metabolomic analysis of serum samples

Serum sample preparation followed our previous study [11], using tamoxifen and cholic acid-d4 as internal standards. To ensure the stability and reproducibility of data acquisition, quality control (QC) samples were prepared by mixing equal aliquots (5 μL) of each sample. Untargeted metabolomic analysis of serum samples was conducted using an Agilent 1260 Infinity LC system (SN: DEAEQ48900) and an Agilent 6545 Q-TOF mass

spectrometer (SN: SG22202E101), equipped with an ESI source (Santa Clara, CA, USA). The LC and MS conditions used in the metabolomic study are detailed in Tables S5 and S6.

2.9. Gut microbiota analysis

Bacterial DNA extraction from fecal samples in mice, PCR amplification, and sequencing were performed according to the standard procedure of Novogene Co., Ltd., as previously described [30]. Detailed experimental protocols and analytical pipelines are provided in the Supplementary Material.

2.10. Metorigin analysis

The Metorigin platform was employed for traceability analysis of differential metabolites and integrative analysis of the gut microbiome and serum metabolome [31]. Specifically, Metorigin's deep analysis module was applied for origin-based metabolite pathway enrichment analysis (MPEA) and Bio-Sankey network visualization, both accessible on the official website.

2.11. SCFA analysis

SCFAs in fecal samples were extracted and derivatized according to a previously reported method [32]. The preparation process of SCFAs and conditions for GC-MS analysis are detailed in the Supplementary Material. Quantification of SCFAs was performed using external calibration curves generated from peak areas of SCFA standards.

2.12. Determination of gene expression using qPCR

Total RNA was extracted from liver and colon tissues using the TransZol Up (TransGen Biotech, Shanghai, China) reagent and reverse-transcribed into cDNA using the SweScript All-in-One RT SuperMix (Servicebio, Wuhan, China). Then, PCR reactions were conducted using the MonAmp SYBR Green qPCR Mix (Monad Biotech, Shanghai, China), with GAPDH serving as an internal reference. The gene primers are listed in Table S7. The mRNA expression was calculated using the $2^{-\Delta\Delta CT}$.

2.13. Statistical analysis

The metabolomic data were processed according to the methodology in our previous study [11]. Data are expressed as the mean ± standard deviation (SD). Statistical comparisons between groups were performed using Student's *t*-test, with $P < 0.05$ considered statistically significant. Graphs were generated using GraphPad Prism 9.

3. Results

3.1. Chemical composition profiling of LBTE

To characterize the primary chemical constituents of LBTE, the levels of total polysaccharides, total polyphenols, total flavonoids, total free amino acids, and total soluble sugars were quantitatively assessed. Among these components, total flavonoids and total polyphenols exhibited notably high content (Figure S3), indicating that these constituents may significantly contribute to the therapeutic potential of LBTE. The total ion chromatogram (TIC) of LBTE is presented in Figure S4, providing the comprehensive chemical fingerprint of LBTE. A total of 34 compounds were preliminarily identified by comparison with the database, including alkaloids, catechins and flavonoids, with flavonoids representing the largest proportion of 30 compounds. The detailed information on these compounds is provided in Table S8.

3.2. Network pharmacology analysis and potential active ingredients identification

To elucidate how these components exert antidiabetic effects, network pharmacology analysis was performed. A total of 140 potential targets associated with LBTE were identified from the SwissTargetPrediction database. Concurrently, 2051 targets related to T2D were obtained from the disease-related databases. After crossing these targets, 62 overlapping targets were found, suggesting their potential involvement in the antidiabetic effects of LBTE (Figure 1A). Core compounds were selected through network topology analysis based on degree centrality values and included quercetin, kaempferol, luteolin, genistein, etc. Subsequent analysis of the 62 intersection targets identified the top 10 hub genes based on degree values: AKT1, TNF, EGFR, SRC, ESR1, PTGS2, MMP9, GSK3B, KDR, and IGF1R (Figure 1B). These hub genes were considered key therapeutic targets for LBTE in the treatment of T2D. To elucidate the biological relevance of these targets, GO and KEGG pathway enrichment analyses were conducted, and the top 10 GO terms and top 20 KEGG pathways are shown in Figure 1D-E. Notably, the PI3K-Akt signaling pathway, insulin resistance, and MAPK signaling pathway emerged as key pathways implicated in T2D pathogenesis, with AKT1, TNF, and GSK3B identified as central regulatory nodes. Additionally, a core compound-target-pathway network was constructed to visualize the multi-target and multi-pathway interactions of the core compounds (Figure 1C). The network revealed that each core compound potentially regulates multiple targets, collectively contributing to the modulation of metabolic and signaling pathways relevant to T2D.

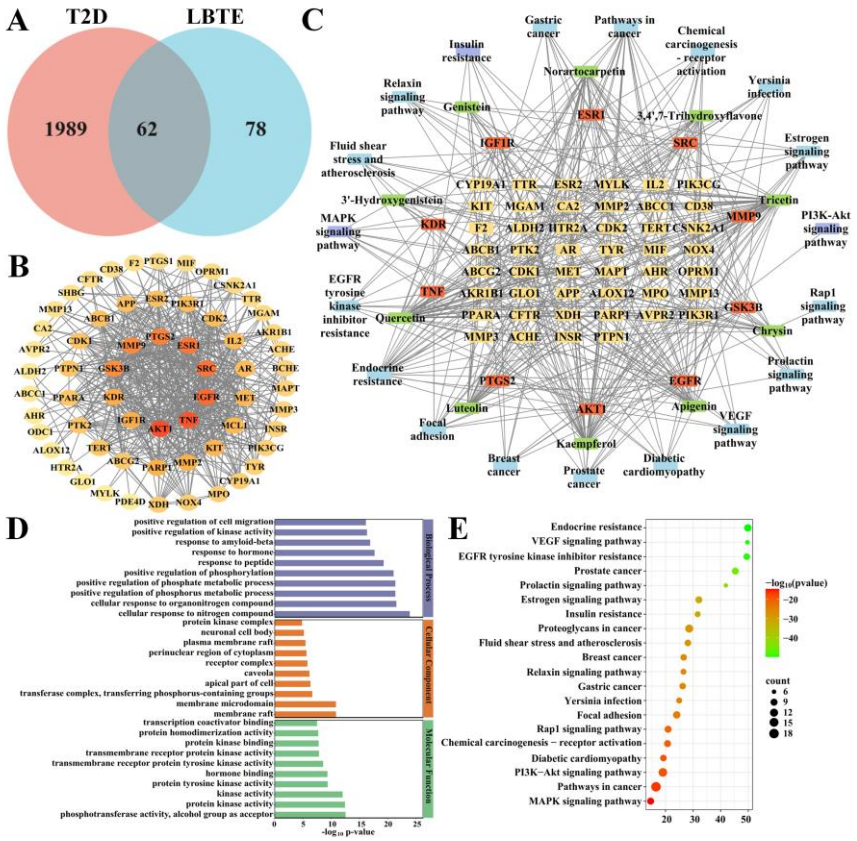


Figure 1. Network pharmacology analysis of Liubao tea extract (LBTE) intervening type 2 diabetes (T2D). (**A**) Venn diagram of the intersection targets of LBTE and T2D. (**B**) PPI (Protein-protein interaction) network. Color depth indicates the target degree. (**C**) Core compounds-targets-pathways network. The light blue, green, purple, yellow, and red indicate KEGG pathways, top 10 compounds, key KEGG pathways, targets, and top 10 targets, respectively. (**D**) GO enrichment analysis. (**E**) KEGG pathway analysis.

Subsequently, four potential active ingredients including quercetin, luteolin, genistein, and kaempferol in LBTE were successfully identified by matching their exact mass, mass error, retention time, and fragmentation patterns with those of chemical standards analyzed under identical conditions (Table S9, Figure S5).

Based on the network pharmacology results, AKT1, TNF, and GSK3B were identified as key targets and subsequently selected for molecular docking analysis. As summarized in Table S10, the docking scores (S score) and predicted binding interactions between the core compounds (quercetin, luteolin, genistein, and kaempferol) and the target proteins are presented. The docking results demonstrated favorable binding conformations and strong affinities (Figure S6). These findings support the hypothesis that LBTE exerts its antidiabetic effects through interactions with multiple targets, particularly involving AKT1, TNF, and GSK3B.

3.3. Quantification of potential ingredients in LBTE

Each component was validated by comparing retention time and mass spectral fragmentation data of chemical standards and their contents were quantified using an external calibration curve based on peak area (Figure 2). The concentrations of caffeine, genistein, naringin, quercetin, luteolin and kaempferol in LBTE were determined to be 30.1 ± 1.8, 1.04 ± 0.05, 0.47 ± 0.07, 1.2 ± 0.02, 0.62 ± 0.12, and 0.76 ± 0.01 mg/g, respectively. These results indicate that LBTE is rich in flavonoids and alkaloids, which may contribute to its antidiabetic effects.

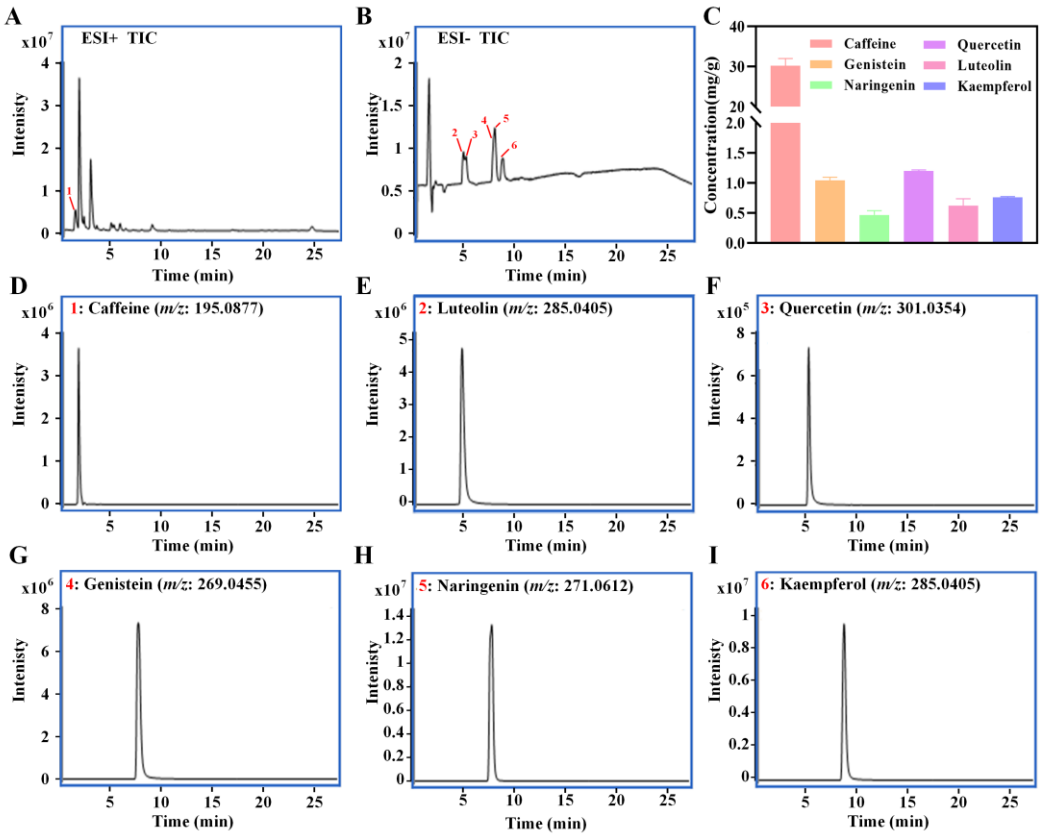


Figure 2. The quantification of potential ingredients in LBTE. (**A, B**) The total ion chromatogram (TIC) of standards detected by LC-MS in the ESI+ and ESI- modes, respectively. (**C**) The concentrations of potential ingredients in LBTE. The extracted ion chromatogram of reference standards: caffeine (**D**), luteolin (**E**), quercetin (**F**), genistein (**G**), naringin (**H**), and kaempferol (**I**).

3.4. Amelioration of LBTE on T2D mice

As shown in Figure 3A, the body weight of T2D mice was significantly lower than that of the NC group between weeks 6 and 9. Treatment with LBTE and metformin further reduced body weight compared to the MC group, with a significant reduction observed in the high-dose LBTE group ($P < 0.05$). These results suggest that LBTE may partially exert its metabolic benefits in T2D mice through weight modulation.

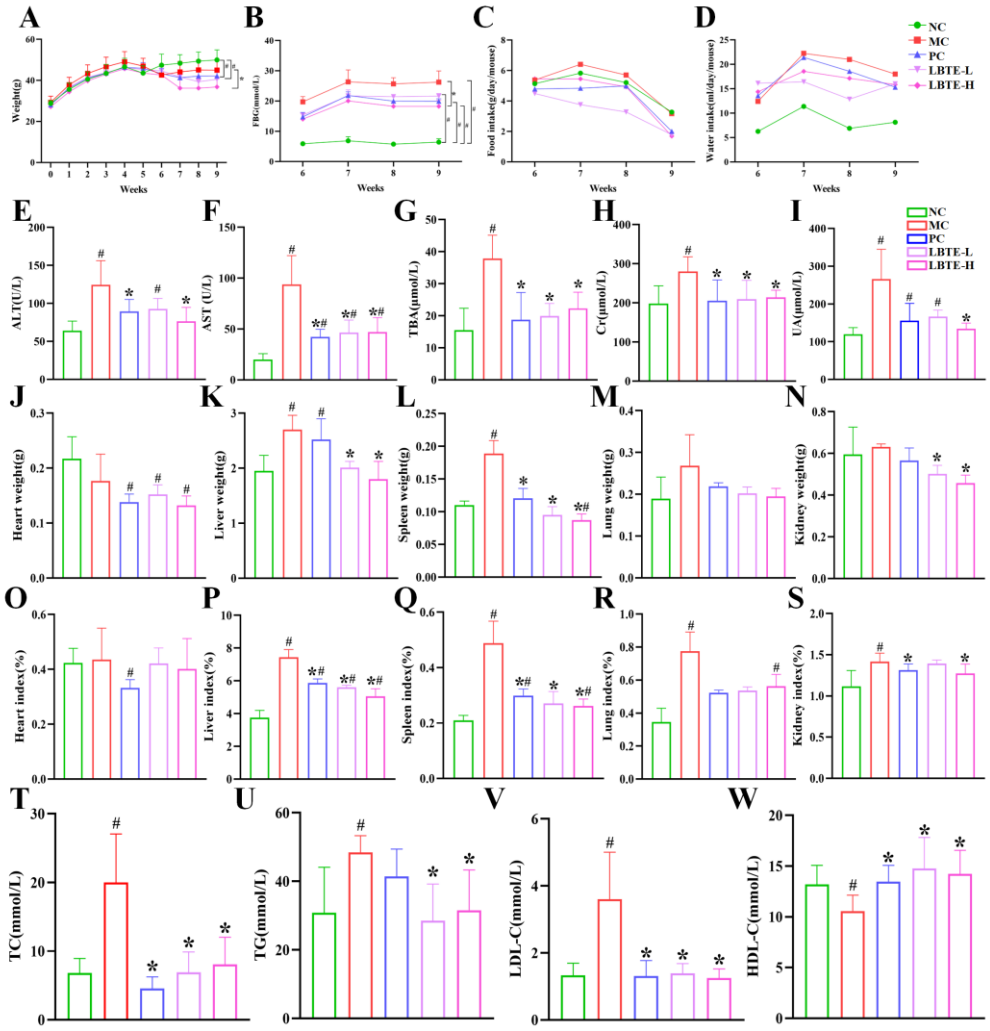


Figure 3. LBTE showed improvement effect on T2D mice. (**A**) Body weight. (**B**) Fasting blood glucose (FBG). (**C**) Food intake. (**D**) Water intake. (**E**) ALT, (**F**) AST, (**G**) TBA, (**H**) Cr, (**I**) UA, (**J**) Heart weight, (**K**) Liver weight, (**L**) Spleen weight, (**M**) Lung weight, (**N**) Kidney weight, (**O**) Heart index, (**P**) Liver index, (**Q**) Spleen index, (**R**) Lung index, (**S**) Kidney index, (**T**) TC, (**U**) TG, (**V**) LDL-C, and (**W**) HDL-C. NC, normal-chow diet; MC, high-fat diet (HFD); PC, HFD + Metformin (200 mg/kg); LBTE-L, HFD + LBTE (200 mg/kg); LBTE-H, HFD + LBTE (400 mg/kg). Data are expressed as mean ± standard deviation (SD) (n = 5). $^{\#}P < 0.05$ compared with the NC group; $^{*}P < 0.05$ compared with the MC group.

While the differences in food and water intake were not statistically significant, a decreasing trend in food consumption in the LBTE-treated groups suggests a possible influence of LBTE on appetite. (Figure 3C-D) FBG levels were notably reduced following LBTE administration, particularly in the high-dose group ($P < 0.05$). Interestingly, FBG levels in the PC group were comparable to those in the LBTE-L group and did not show a significant reduction relative to the MC group (Figure 3B). The comparison of two different administered dose methods revealed nearly identical FBG levels in both groups (Figure S7A). Further evaluation of different dosing regimens revealed that triple dosing

produced a more pronounced glucose-lowering effect than single dosing (Figure S7B-C), suggesting that hypoglycemic efficacy depends on dosing frequency and drug exposure duration, consistent with the reported elimination half-life (~5 hours) of metformin [33], it could be hypothesized that the hypoglycemic efficacy of metformin and LBTE was strongly influenced by dosing frequency and duration of exposure. Serum lipid analyses showed that the levels of TC, TG, LDL-C, and HDL-C were significantly altered in the MC group compared to the NC group ($P < 0.05$) (Figure 3T-W). LBTE treatment significantly reversed these changes ($P < 0.05$).

Histopathological examination revealed that the MC group exhibited abnormal hepatic architecture, lipid droplet accumulation, and inflammatory infiltration compared to the NC group, whereas LBTE markedly ameliorated these pathological changes (Figure 4A-B). Adipose tissue also revealed fat accumulation in the MC group, which was alleviated by LBTE, particularly at high doses (Figure 4C). Consistently, liver weight and index were significantly elevated in the MC group but significantly reduced following LBTE treatment ($P < 0.05$) (Figure 3K, P). The levels of ALT, AST, and TBA were significantly elevated in the MC group compared with the NC group and normalized upon LBTE intervention ($P < 0.05$) (Figure 3E-G), suggesting hepatoprotective effects of LBTE for T2D mice. Moreover, LBTE treatment significantly reversed the changes in kidney weight and index observed in the MC group ($P < 0.05$) (Figure 3N, S). Serum levels of Cr and UA were also markedly elevated in the MC group compared to the NC group, indicating renal dysfunction, while LBTE intervention significantly lowered Cr and UA levels ($P < 0.05$) (Figure 3H-I). Although no obvious pathological changes were observed in kidney tissues across all groups (Figure 4F), the biochemical improvements suggested that LBTE conferred renal protective effects. Additionally, spleen weight and index were significantly elevated in MC group and dose-dependently normalized following LBTE treatment ($P < 0.05$, Figure 3L, Q), suggesting a potential immunomodulatory effect. While no significant changes were observed in lung weight and index (Figure 3M, R), histological analysis revealed that LBTE alleviated alveolar wall thickening and inflammatory infiltration present in T2D mice (Figure 4E), suggesting a protective effect against pulmonary inflammation. Finally, no significant differences in heart weight or index were observed (Figure 3J, O), and no pathological changes were noted in heart tissues across all groups (Figure 4D), suggesting that neither T2D nor LBTE treatment had a significant impact on cardiac morphology during the study period. In the colon, the MC group showed disrupted colonic tissue structure and increased inflammatory infiltration, whereas LBTE treatment effectively restored colon integrity and alleviated the inflammatory state (Figure 4G), highlighting a protective effect on intestinal barrier function. In summary, LBTE exerted multifaceted protective effects in T2D mice, including improvements in glycemic control, lipid profiles, liver and kidney function, as well as attenuation of inflammation and tissue damage across multiple organs, thereby supporting its therapeutic potential in metabolic disease management.

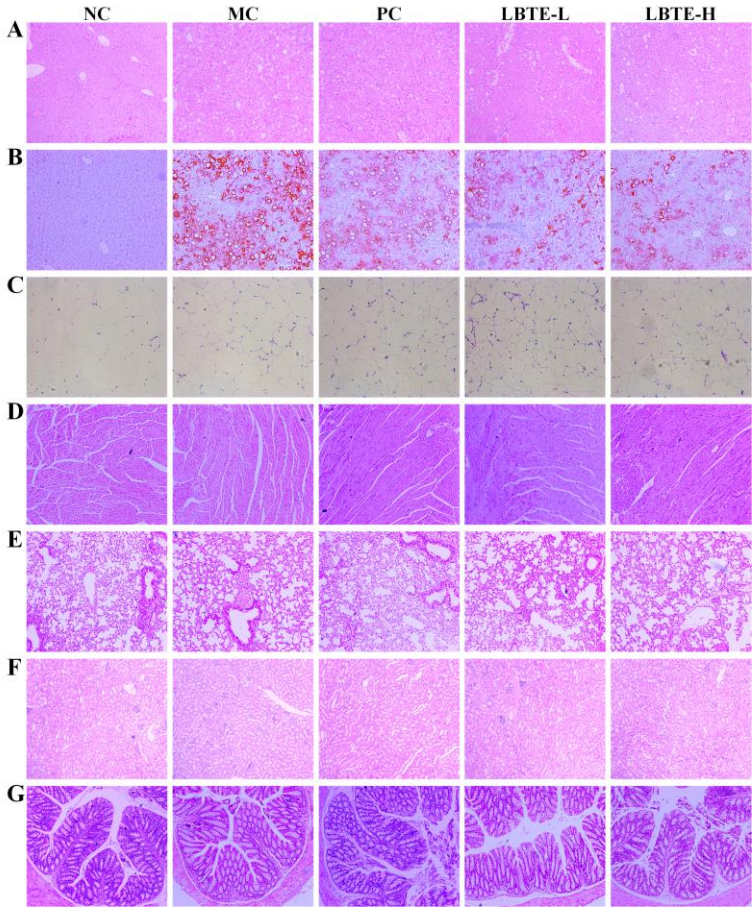


Figure 4. Effects of LBTE administration on the organ histopathologic changes of mice. (**A**) H&E staining of liver tissue (200 ×). (**B**) Oil Red O staining of liver tissue (100 ×). (**C**) H&E staining of adipose tissue (200 ×). (**D**) H&E staining of heart tissue (100 ×). (**E**) H&E staining of lung tissue (100 ×). (**F**) H&E staining of kidney tissue (200 ×). (**G**) H&E staining of colon tissue (100 ×).

3.5. Influence of LBTE treatment on the serum metabolic profiles of T2D mice

To evaluate the metabolic impact of LBTE on T2D mice, serum untargeted metabolomics was performed. As shown in Figure S8, the TIC of QC samples exhibited substantial overlap, indicating excellent instrument performance and validating the reliability of the acquired data. Subsequently, an orthogonal partial least squares-discriminant analysis (OPLS-DA) revealed clear clustering and separation across all groups. As expected, samples from the MC group were distinctly separated from those of the NC group, reflecting pronounced metabolic disturbances induced by T2D. Notably, the metabolic profile of the LBTE-H group diverged significantly from the MC group and trended toward the NC group (Figure 5A-B), suggesting a restorative effect of LBTE on T2D-associated metabolic dysfunction. Model validity and predictive accuracy were evaluated using R^2 and Q^2 values, and permutation tests (n = 200) further confirmed the robustness of the OPLS-DA model and excluded overfitting (Figure 5C-D). Key differential metabolites were screened based on the OPLS-DA models using the following criteria: fold change (FC) > 1.5 or < 0.67, variable importance in projection (VIP) > 1, and $P < 0.05$. The differential metabolites were classified into several chemical categories, mainly including amines, prenol lipids, sterol lipids, fatty acids (FAs), glycerophospholipids (GPs), sphingolipids (SPs), glycerolipids, lipids, amino acids (AAs) and xanthines (Figure 5E-G). Among these, GPs accounted for the largest fraction, exceeding 50% of all differential metabolites, followed by FAs and SPs.

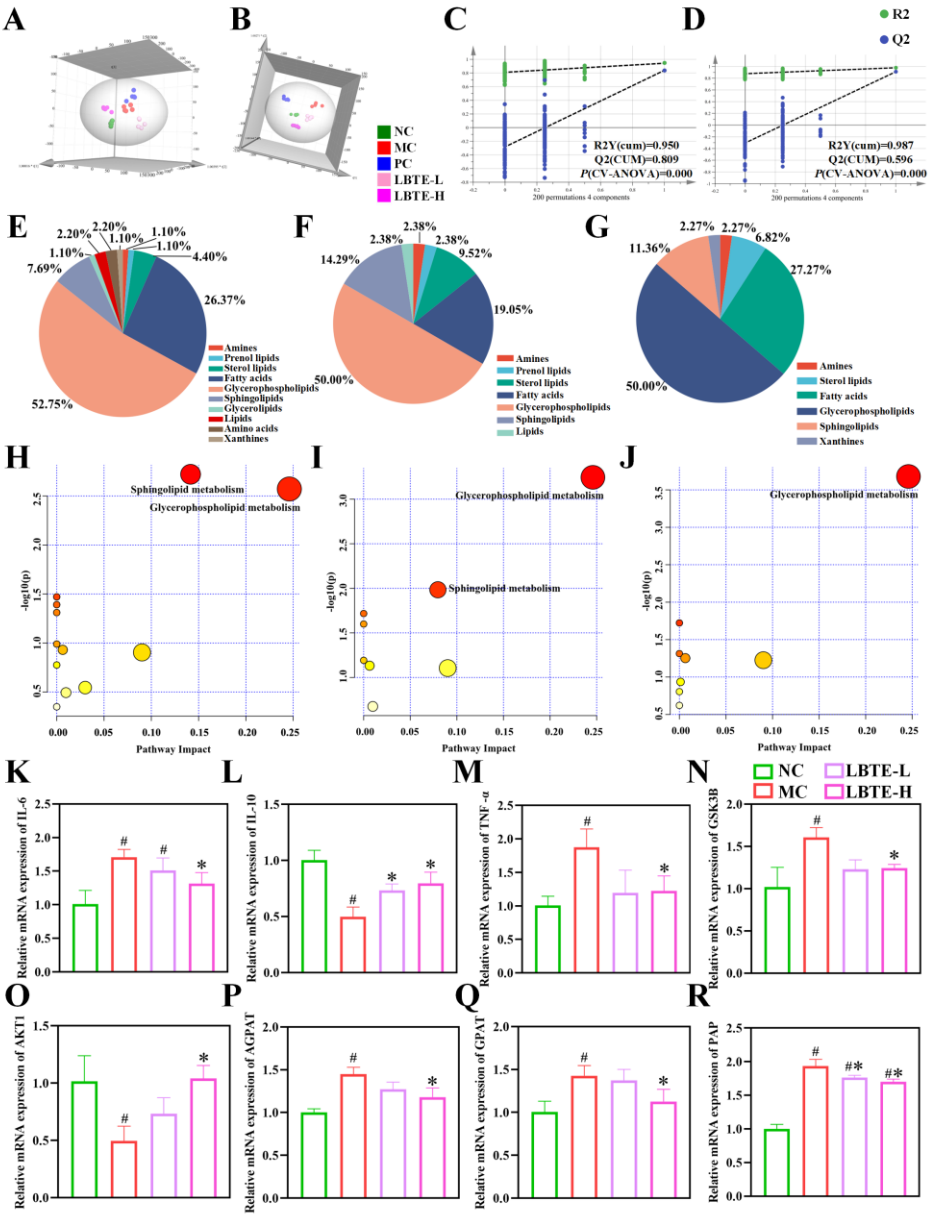


Figure 5. Effects of the serum metabolic profiling and the gene expression level of *IL-6*, *IL-10*, *TNF-α*, *GSK3B*, *AKT1*, *AGPAT*, *GPAT*, and *PAP* in mice treated with LBTE. (**A, B**) OPLS-DA of serum metabolic profiling among the five groups in both ESI modes, respectively. (**C, D**) OPLS-DA model permutation test for both ESI modes, respectively. (**E-G**) The composition ratio of serum differential metabolites in the NC vs. MC groups, LBTE-L vs. MC groups, and LBTE-H vs. MC groups, respectively. (**H-J**) The analysis of metabolic pathways of serum differential metabolites in the NC vs. MC groups, LBTE-L vs. MC groups, and LBTE-H vs. MC groups, respectively. The relative mRNA expression level of *IL-6* (**K**), *IL-10* (**L**), *TNF-α* (**M**), *GSK3B* (**N**), *AKT1* (**O**), *AGPAT* (**P**), *GPAT* (**Q**), and *PAP* (**R**) in the liver tissue. Data are displayed with mean ± SD (n = 5). $^{\#}$ $P < 0.05$ compared with the NC group; * $P < 0.05$ compared with the MC group.

To disclose the potential mechanisms underlying T2D pathogenesis and the therapeutic effects of LBTE, metabolic pathway enrichment analysis was conducted based on serum differential metabolites. In T2D mice, obvious dysregulation was observed in both sphingolipid (SP) and glycerophospholipid (GP) metabolism, with statistical thresholds of $P < 0.05$ or impact factor (IF) > 0.1 (Figure 5H). Remarkably, these metabolic disturbances were attenuated following LBTE intervention (Figure 5I-J), suggesting that

modulation of these pathways could be involved in the therapeutic effects of LBTE. Further analysis identified 16 shared serum differential metabolites across four groups (Figure S9). To assess their diagnostic and therapeutic relevance, ROC analysis was employed, with stringent screening criteria of AUC > 0.95 and FC > 5 to minimize false positives. Among these, 13 metabolites demonstrated excellent discriminatory power between the NC and MC groups, with AUC values reaching up to 1.00, thereby underscoring their potential as robust diagnostic biomarkers for T2D (Figure S10A-M). ROC analysis of the differential metabolites from comparing the MC group with the LBTE-L and LBTE-H groups identified four and five metabolites, respectively, with AUC values exceeding 0.95 (Figure S10N-V). Notably, metabolites such as PS 38:0, PC 40:7, PE 38:2, PE 41:3, and 1-methylhistamine, mainly derived from GPs and amines, were considered as the key indicators of LBTE's therapeutic benefits in T2D. Consequently, LBTE exerted its anti-T2D effects primarily through the modulation of GP metabolism.

3.6. Regulation of LBTE on expression of key genes involved in inflammatory response, glucose and lipid metabolism pathways

As depicted in Figure 5K-R, the mRNA expression levels of *IL-10* and *AKT1* were significantly decreased in the MC group compared to the NC group, whereas the expression levels of *IL-6*, *TNF-α*, *GSK3B*, *AGPAT*, *GPAT*, and *PAP* were significantly increased ($P < 0.05$). Notably, the administration of LBTE significantly reversed these alterations, restoring the gene expression profiles close to those of the NC group ($P < 0.05$). The results indicated that LBTE alleviated T2D by suppressing inflammation and modulating key pathways involved in glucose utilization and lipid synthesis, thereby improving metabolic imbalances.

3.7. LBTE administration modulated the gut microbiota profiles in T2D mice

To evaluate the impact of LBTE on gut microbial ecology, 16S rRNA sequencing was conducted on fecal samples. A total of 176 amplicon sequence variants (ASVs) were identified across all samples, with 165 ASVs unique to the MC group and 163 ASVs unique to the LBTE-H group (Figure 6B), highlighting distinct microbial signatures between disease and treatment conditions. Analysis of α-diversity indexes, including chao1, observed_species, pielou_e, and shannon indexes, revealed no significant differences between the NC and MC groups as well as between the MC and LBTE groups (Figure 6D-G). However, the α-diversity indexes in the LBTE-H group were more similar to those in the NC group, indicating a partial restoration of microbial richness and evenness following LBTE treatment. β-diversity analysis of gut microbiota, assessed by OPLS-DA (Figure 6I) and hierarchical clustering (Figure 6H), revealed clear distinctions between the NC and MC groups, as well as between the MC and LBTE-H groups, with notable proximity in microbial profiles between the NC and LBTE-H groups. These results indicate that LBTE administration remodeled the gut microbial community structure disrupted by T2D. At the phylum level (Figure 6A), the gut microbiota was predominantly composed of *Firmicutes*, *Bacteroidetes*, *Verrucomicrobiota* and *Patescibacteria*. The MC group exhibited an increased abundance in *Firmicutes* and a decreased abundance in *Bacteroidetes* compared to the NC and LBTE-H groups. LBTE treatment partially reversed this dysbiosis in T2D mice, restoring a microbial composition more similar to healthy mice.

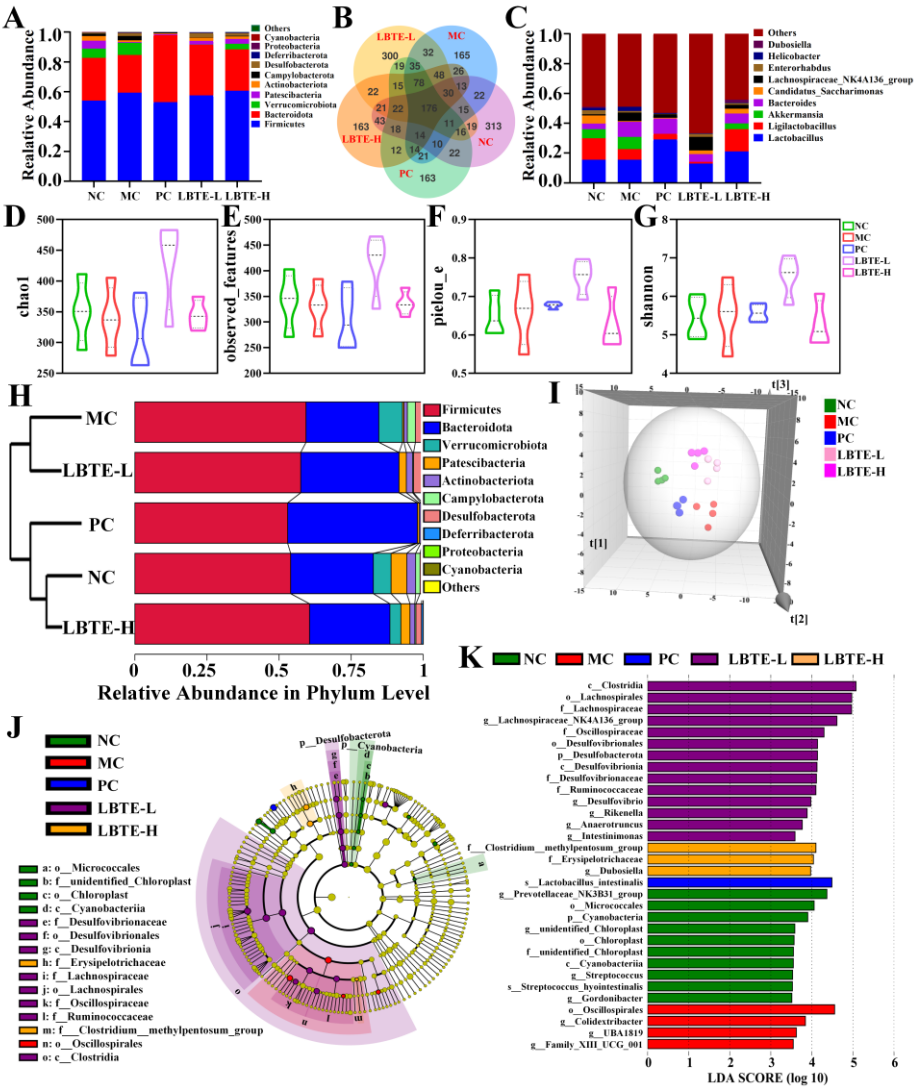


Figure 6. Remodeling effects of LBTE administration on the gut microbiota in T2D mice. (**A, C**) Relative abundance at the phylum and genus levels, respectively. (**B**) Venn diagram of ASVs identified in the gut microbiota. (**D-G**) Alpha diversity of gut microbiota evaluated by chao1, observed_species, pielou_e, and shannon indexes. (**H**) Hierarchical clustering tree analysis. (**I**) Beta diversity of gut microbiota evaluated by weighted OPLS-DA score plot. (**J**) Cladogram generated from LEfSe analysis. (**K**) LDA score derived from LEfSe analysis.

At the genus level (Figure 6C), *Akkermansia*, *Lactobacillus*, *Ligilactobacillus*, and *Bacteroides* were dominant across all groups. The relative abundance of *Lachnospiraceae_NK4A136_group*, *Akkermansia*, *Bacteroides*, *Lactobacillus*, and *Helicobacter* was increased, while the *Ligilactobacillus*, *Candidatus_Saccharimonas*, and *Enterorhabdus* were decreased in the MC group. These alterations were reversed following LBTE-H treatment (Figure S11A-H). Further, Linear Discriminant Analysis Effect Size (LEfSe) analysis with an LDA threshold of three was conducted to reveal specific bacterial changes. The MC group was enriched in *Oscillospirales* at the order level, the NC group in *Micrococcales*, *Chloroplast*, and *Cyanobacteriia*, while the LBTE-H group was characterized by *Erysipelotrichaceae* and *Clostridium_methylpentosum _group* (Figure 6J-K). To assess functional shifts in microbial metabolism, PICRUSt2 was employed for predictive metagenomic analysis. As shown in Figure S11I, the top 10 most abundant functional proteins were primarily involved in bacterial material transport and carbohydrate metabolism. Notably, genes encoding K07024 (sucrose-6-phosphatase, SPP) and K15634 (probable phosphoglycerate

mutase, gpmB) were down-regulated in the MC group but restored following LBTE treatment, suggesting that LBTE may enhance microbial-mediated carbohydrate metabolism. Collectively, LBTE treatment reshaped the gut microbiota in T2D mice by restoring microbial balance and diversity, enriching beneficial taxa, and enhancing predicted carbohydrate metabolism. These findings highlight the microbiota-mediated mechanisms underlying LBTE's antidiabetic effects.

3.8. Metorigin tracing analysis of differential metabolites

In the comparison between the NC and MC groups, 136 differential metabolites associated with T2D were identified (Figure S12B-C). MPEA revealed that these metabolites were involved in 13 co-metabolism pathways (Figure S12D). Among them, SP and GP metabolism (log0.05 $P > 2$) were identified as the most significantly enriched pathways in the co-metabolism between gut microbiota and the hosts, indicating their pivotal role in the pathogenesis of T2D (Figure S12A). In the GP metabolism-related metabolic reaction R01320, PC 40:7 was identified as the key metabolite, with *Helicobacter* being the primary associated genus, showing a strong positive correlation (Figure S12E). Similarly, PS 38:0 was the major metabolite in reaction R01800, which involved four bacterial genera related to GP metabolism. Among these, *Bacteroides*, *Akkermansia*, and *Helicobacter* exhibited positive correlations with PS 38:0, whereas *Ligilactobacillus* showed a negative correlation (Figure S12F). In addition, three key metabolites including sphingosine, sphinganine, and phytosphingosine were identified in the metabolic reactions R01494, R06518, and R06528, respectively, related to SP metabolism, underscoring their contribution to lipid dysregulation in T2D (Figure S13A-C).

In the comparison between the MC and LBTE-L groups, 70 differential metabolites were identified (Figure S14B-C). MPEA revealed that nine significantly enriched co-metabolic pathways, with GP metabolism being the most notably modulated (Figure S14A, D). Similarly, in the comparison between the MC and LBTE-H groups, 68 differential metabolites were identified (Figure S15B-C). MPEA indicated that modulation of seven co-metabolic pathways was associated with co-metabolism pathway databases, among which GP metabolism was most significantly affected (Figure S15A, D). Consistently, PC 40:7 and *Helicobacter* remained central elements in metabolic reaction R01320, which showed a positive correlation (Figure S14E, S15E). Moreover, PS 38:0 and its associated genera (*Bacteroides*, *Akkermansia*, *Helicobacter*, and *Ligilactobacillus*) were repeatedly highlighted in reaction R01800, further supporting their involvement in GP metabolism (Figure S14F, S15F). Therefore, LBTE exerted its anti-T2D effects primarily by modulating GP metabolism, likely mediated by restructuring the abundance of key microbiota, thereby restoring host-microbiota metabolic balance to alleviate T2D.

3.9. LBTE enhanced the intestinal barrier function by promoting SCFA production and regulating GPCR gene expression

To evaluate the impact of LBTE on gut microbial metabolism, fecal SCFAs were quantitatively analyzed. The levels of three major SCFAs, as well as the total SCFA content, were significantly elevated in the NC and LBTE-treated groups compared to the MC group ($P < 0.05$) (Figure 7A), suggesting that LBTE facilitated the recovery of gut microbial metabolic activity impaired by T2D. In the MC group, the mRNA expression levels of *GPR41* and *GPR109A* in both colon and liver tissues were significantly down-regulated compared to the NC group, whereas LBTE treatment significantly upregulated the expression of these receptors, with more pronounced effects observed in the high-dose group ($P < 0.05$) (Figure 7D-G). In addition, the mRNA expression levels of tight junction proteins, *ZO-1* and *Occludin*, were significantly lower in the MC group compared to the NC group, indicating compromised intestinal barrier function. LBTE treatment significantly restored

the mRNA expression levels of these proteins, thereby effectively improving intestinal barrier function ($P < 0.05$) (Figure 7B-C). Collectively, these results demonstrate that LBTE exerted protective effects in T2D mice by promoting SCFA production and enhancing the expression of GPCRs and tight junction proteins, thus contributing to the restoration of intestinal barrier function.

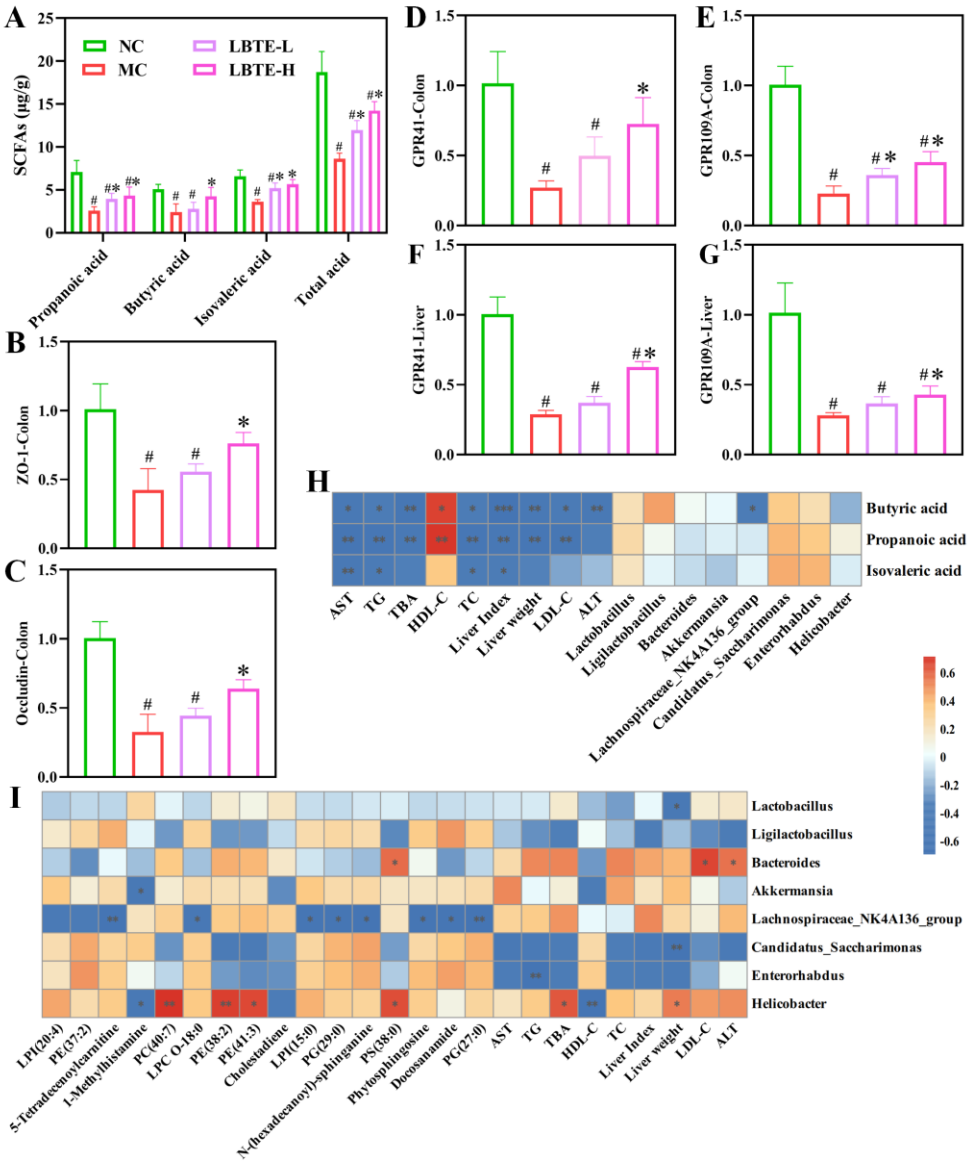


Figure 7. Regulatory effect of LBTE on fecal SCFAs and the intestinal barrier function in T2D mice. (**A**) The levels of SCFAs. (**B-E**) The mRNA levels of *ZO-1*, *Occludin*, *GPR41*, and *GPR109A* in the colon tissue. (**F-G**) The mRNA levels of *GPR41* and *GPR109A* in the liver tissue. (**H**) The correlation analysis between SCFAs and gut microbiota or biochemical indicators. (**I**) The correlation analysis between gut microbiota and differential metabolites or biochemical indicators. In panel A-G, data are displayed with mean ± SD (n = 5). $^{\#}$ P <0.05 compared with the NC group; * $P < 0.05$ compared with the MC group. In panel H-I, significant correlations are marked by * $P < 0.05$, and ** $P < 0.01$ in the heatmap. Red and blue squares indicate positive and negative correlations, respectively.

3.10. Correlation analysis

Correlation analyses were conducted to elucidate the interactions among T2D-related biochemical indicators, key metabolites, key bacterial genera, and SCFA levels. As shown in Figure 7I, the relative abundances of *Helicobacter* showed a significant positive

correlation with those of PE 38:2, PE 41:3, PS 38:0, and PC 40:7 ($P < 0.05$). Moreover, the relative abundances of *Bacteroides* exhibited significant positive correlations with the levels of LDL-C and ALT ($P < 0.05$). The relative abundances of *Helicobacter* exhibited significant positive correlations with the levels of TBA and liver weight, while presenting significant negative correlations with the levels of HDL-C ($P < 0.05$). However, the *Ligilactobacillus*, *Candidatus_Saccharimonas*, and *Enterorhabdus* showed the opposite trends, displaying negative correlations with these metabolites and biochemical indicators. As shown in Figure 7H, the levels of SCFAs were negatively correlated with the relative abundances of *Helicobacter*, *Akkermansia*, and *Bacteroides*, while positively correlated with the relative abundances of *Candidatus_Saccharimonas*, *Enterorhabdus*, and *Ligilactobacillus*. Moreover, SCFA levels were negatively correlated with all T2D-related biochemical indicators, except HDL-C, which showed a positive correlation. These findings further suggest that gut microbiota contribute to the amelioration of metabolic disorders and liver dysfunction in T2D by enhancing SCFA production.

3.11. LBTE alleviated T2D pathology depending on gut microbiota

To confirm whether gut microbiota was involved in the improvement effects of LBTE on T2D, a pseudo-germ-free mouse model was established using a cocktail of broad-spectrum antibiotics. After antibiotic treatment, the α-diversity indexes including chao1, observed_species, pielou_e, and shannon of both the MA and LBTEA groups, were significantly lower and close to zero compared to the MC group ($P < 0.05$), confirming the successful establishment of the pseudo-germ-free mouse model (Figure 8A-D). NMDS analysis further disclosed that the gut microbiota compositions of the MA and LBTEA groups were highly similar, yet distinctly separated from that of the MC group (Figure 8E).

In addition, antibiotic intervention significantly altered the microbial community, transforming it from a highly diverse community to one dominated by *Proteobacteria*. Compared with the MC group, the abundance of *Firmicutes* and *Bacteroidota* significantly decreased, while *Proteobacteria* sharply increased in the MA and LBTEA groups (Figure 8F). Importantly, LBTE treatment failed to restore the gut microbiota profiles in the presence of antibiotic intervention, suggesting a loss of its therapeutic efficacy in the absence of a functional microbiota. We further evaluated the impact of these microbiota changes on SCFA production. As shown in Figure S16A, propionic acid levels were significantly lower in the MA and LBTEA groups compared to the MC group ($P < 0.05$), whereas butyric acid and isovaleric acid were almost undetectable. Histological examination revealed that, similar to the MC group, mice in both the MA and LBTEA groups exhibited crypt damage and inflammatory cell infiltration in colonic tissues (Figure S16B). The inability of LBTE to ameliorate colonic histopathological abnormalities was closely associated with the reduced SCFA levels following antibiotic treatment.

Regarding physiological parameters, the body weight of mice in the MC group continued to decrease throughout the experiment, and body weight trends in the MA and LBTEA groups mirrored those of the MC group, with no significant differences observed (Figure 8G). Meanwhile, the FBG levels were persistently elevated across all three groups, with no significant differences between them, indicating that the hypoglycemic effect of LBTE was abolished after antibiotic intervention (Figure 8H). Although no significant difference in water intake among the three groups of mice (Figure 8J), the food intake in the MA and LBTEA groups decreased compared to the MC group (Figure 8I), likely due to the profound disruption of gut microbiota. There were no significant differences in TC, TG, LDL-C, and HDL-C levels between the MA group and the LBTEA group compared to the MC group (Figure 8K-N). This indicated that the modulatory effects of LBTE on lipid metabolism disorders were abolished after gut microbiota disruption.

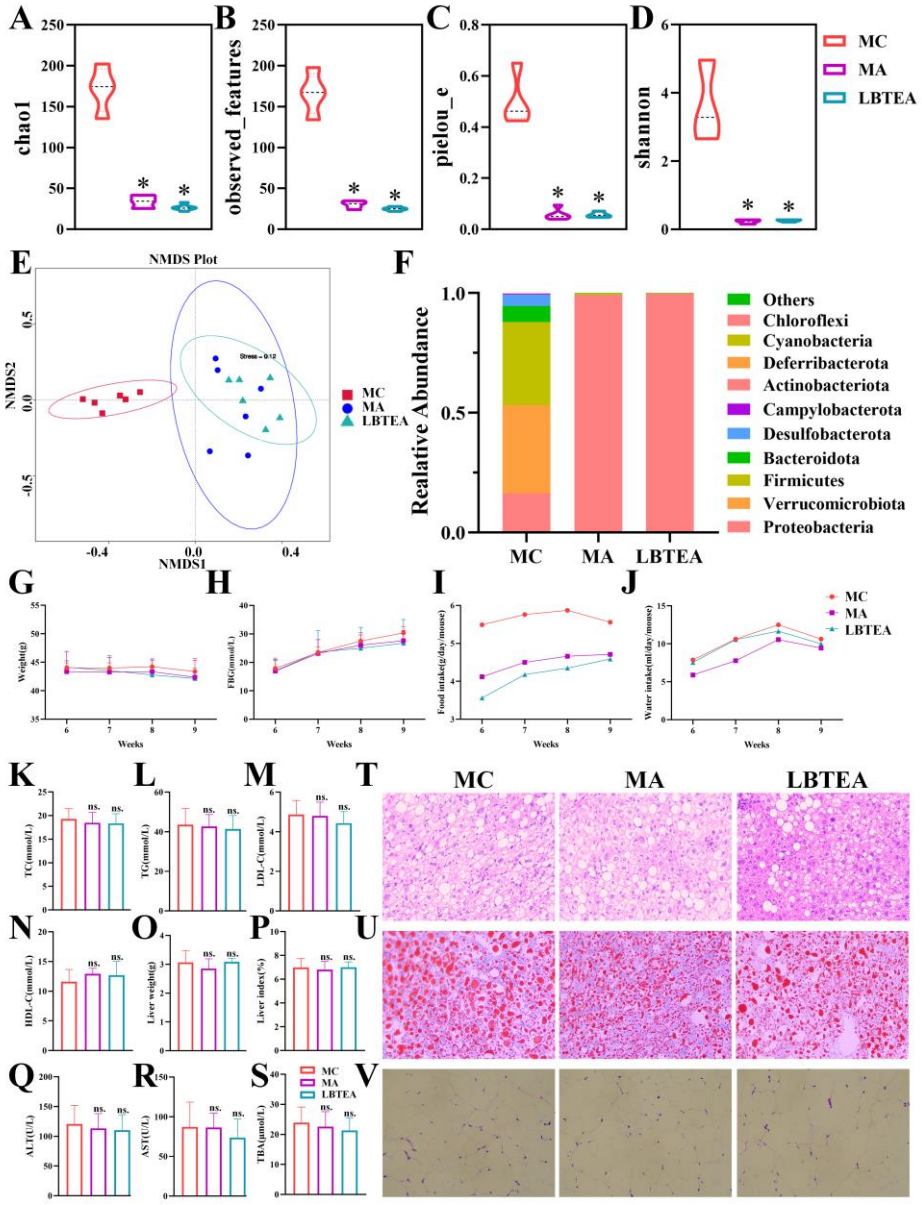


Figure 8. LBTE exerted improvement effect in T2D depending on gut microbiota. (**A-D**) Alpha diversity of gut microbiota evaluated by chao1, observed_species, pielou_e, and shannon indexes. (**E**) Beta diversity of gut microbiota evaluated by weighted NMDS plot. (**F**) Relative abundance at phylum level. (**G**) Body weight. (**H**) FBG. (**I**) Food intake. (**J**) Water intake. (**K**) TC, (**L**) TG, (**M**) LDL-C, (**N**) HDL-C, (**O**) Liver weight, (**P**) Liver index, (**Q**) ALT, (**R**) AST, and (**S**) TBA. (**T**) H&E staining of liver tissue (200 ×). (**U**) Oil Red O staining of liver tissue (200 ×). (**V**) H&E staining of adipose tissue (200 ×). MC, HFD; MA, HFD + antibiotic; LBTEA, HFD + antibiotic + LBTE (400 mg/kg). Data are expressed as mean ± SD (n = 5). * $P < 0.05$ compared with the MC group; $^{ns.}$ $P > 0.05$ compared with the MC group.

Histopathological analysis of adipose tissues further confirmed these findings, revealing that antibiotic intervention reversed the LBTE improvements in lipid accumulation induced by T2D (Figure 8V). Similarly, no significant differences were observed in the liver weight, liver index, serum ALT, AST, and TBA levels between the MA, LBTEA, and MC groups (Figure 8O-S). H&E staining and Oil Red O staining of liver tissues showed that the liver tissues of mice in the MC group showed significant lipid accumulation and inflammation, whereas antibiotics combined with LBTE failed to alleviate liver injury in mice with T2D (Figure 8T-U). Therefore, antibiotic intervention effectively

negated the therapeutic benefits of LBTE, resulting in the loss of its ability to improve metabolic disorders, reduce lipid accumulation, and alleviate liver damage. These findings underscore that the therapeutic efficacy of LBTE against T2D is strongly microbiota-dependent, reinforcing the importance of gut–host interactions in metabolic disease modulation.

4. Discussion

This study revealed the potential mechanism of LBTE in improving T2D by integrating bioinformatics analysis, multi-omics technology and *in vivo* experimental verification. Network pharmacology combined with targeted metabolomics revealed that quercetin, luteolin, genistein, and kaempferol were potential bioactive compounds in LBTE, exerting antidiabetic effects by regulating signaling pathways such as PI3K-Akt, insulin resistance, and MAPK. Molecular docking demonstrated that these flavonoids have strong binding affinities to key targets such as AKT1, GSK3B, and TNF-α. Among them, luteolin and quercetin have been shown to improve the disorders of glucose and lipid metabolism [34,35], genistein has both hypoglycemic and insulin resistance-reducing properties [17], and kaempferol reduces the inflammatory response by inhibiting the NF-κB pathway [36], which provided the theoretical basis for the subsequent *in vivo* experiments.

In order to investigate the ameliorative effect of LBTE *in vivo*, studies were conducted in T2D mice, which exhibit T2D-related characteristics consistent with previous studies [37]. In the T2D mouse model, LBTE significantly reduced FBG and improved dyslipidemia, while reversing hepatic lipid accumulation and inflammation, alveolar wall thickening and colonic tissue intestinal barrier damage. Although no significant differences in food intake were observed among the groups, a downward trend in LBTE-treated groups may indicate subtle appetite regulation. Tea polyphenols, including quercetin and kaempferol, have been reported to modulate gut–brain axis activity through the microbiota and its metabolites, which may in turn affect satiety and feeding behavior[38,39]. These findings imply that LBTE may exert mild anorexigenic effects as part of its overall metabolic modulation. In addition, metabolomics further revealed that LBTE exerted its ameliorative effects mainly through the regulation of SP and GP metabolic pathways. Previous studies have highlighted the crucial role of SPs in causing glucose disturbances, as well as abnormal GP metabolism as a factor in the pathophysiology of diabetes [40,41]. The research findings were consistent with these studies, with LBTE being particularly critical in regulating GP metabolism. T2D is a chronic metabolic disease characterized by hyperglycemia and disorders of lipid metabolism [42]. LBTE promoted the conversion of glucose to glycogen in the liver by up-regulating the expression of *AKT1* and down-regulating the expression of *GSK3B*, thereby reducing blood glucose. Meanwhile, glucose undergoes the glycolysis pathway to produce Glycerol-3-phosphate (G-3-P), which is a substrate in GP synthesis pathway [43]. LBTE could block the metabolic flow of G-3-P to diacylglycerol (DAG) by downregulating the expression of related genes involved in the GP synthesis pathway (including *GPAT*, *AGPAT* and *PAP*) [44], thereby reducing the synthesis and accumulation of GP and TG in the liver, and improving dyslipidemia. Metabolic disorders can lead to abnormal inflammation [42], which is often accompanied by lipid accumulation, thereby exacerbating liver injury [45,46]. LBTE significantly reduced the expression levels of *TNF-α* and *IL-6*, while increasing the expression level of *IL-10* in the liver. The protective effect of LBTE on the liver may be related to regulating metabolic disorders and alleviating inflammatory states.

Studies have shown that alterations in the composition of gut microbiota affect the onset of diabetes [47]. The MC group exhibited a higher *Firmicutes* to *Bacteroidetes* (F/B) ratio compared to other groups, which contributed to metabolic disorders and insulin resistance [48]. LBTE reversed the F/B ratio, enriching beneficial bacteria such as

Candidatus_Saccharimonas and *Ligilactobacillus*, while inhibiting the proliferation of harmful bacteria including *Bacteroides*, *Akkermansia* and *Helicobacter*. *Bacteroides* are linked to increased LPS levels and decreased insulin sensitivity, and *Akkermansia* are enriched in T2D samples [49,50]. An increase in *Helicobacter* promotes insulin resistance, accelerating diabetes progression. *Ligilactobacillus* helps improve the function of the intestinal microbiota and intestinal barrier as well as promote carbohydrate metabolism [51]. *Candidatus_Saccharimonas*, an acid-producing bacterium important for maintaining intestinal pH [52]. Previous studies have suggested that the gut microbiota could reshape host metabolism [53]. LBTE regulates GP metabolism by modulating the levels of certain beneficial and harmful gut bacteria. The specific resident bacteria in the gut can metabolize indigestible carbohydrates into various SCFAs molecules [54]. Enzymes like SPP and gpmB play crucial roles in bacterial carbohydrate metabolism [55]. The increased carbohydrate metabolism observed in the LBTE-H group reflected an increase in carbohydrate-utilizing bacteria such as *Candidatus_Saccharimonas* and *Ligilactobacillus*.

As metabolites of intestinal flora, SCFAs are produced in the colon and partially enter the liver through the portal vein [56]. SCFAs help maintain intestinal barrier integrity and regulate host inflammatory responses. LBTE significantly increased the content of fecal SCFAs, among them, butyric acid has been widely proven to enhance intestinal barrier function by upregulating the expression levels of tight junction proteins *ZO-1* and *Occludin* [50]. T2D is usually characterized by insulin resistance, mainly caused directly or indirectly by increased inflammation [57]. SCFA reduces the release of pro-inflammatory factors such as TNF-α, IL-6, and IL-1β by activating signaling pathways mediated by GPR41 and GPR109A receptors [58], thereby synergistically alleviating inflammatory responses and reducing liver injury [59]. Inhibiting inflammation is an important strategy for LBTE treatment of liver injury. Meantime, inflammation can disrupt the insulin signaling pathway and mediate glucose intolerance, with TNF-α further exacerbating metabolic disorders by interfering with the PI3K-Akt signaling pathway [60]. As the core effector molecule of this pathway, AKT promotes glycogen synthesis by inhibiting GSK3B, thereby maintaining blood glucose homeostasis [61]. Elevated levels of serum TG and TC are also important factors in inducing insulin resistance. SCFAs effectively reduce TG and TC levels by inhibiting hepatic adipogenesis and inflammatory cell infiltration [62]. Correlation analysis further confirmed that SCFAs were significantly negatively correlated with lipid indices and liver injury markers, highlighting their metabolic protective effects. The critical role of gut microbiota in mediating the antidiabetic effects of LBTE was further validated in a pseudo-germ-free mouse model. Antibiotic-induced depletion of the gut microbiota abolished the modulatory effects of LBTE on microbial composition, SCFA production, and glucose-lipid metabolism, confirming a microbiota-dependent mechanism.

Nonetheless, this study has certain limitations. The predicted interactions between core compounds (quercetin, luteolin, genistein, and kaempferol) and key protein targets (AKT1, TNF, and GSK3B) were solely based on *in silico* analyses, without experimental validation. Future studies should employ *in vitro* and *in vivo* assays, such as Western blotting or enzyme activity measurements, to substantiate these mechanistic predictions.

5. Conclusions

This study demonstrates that LBTE ameliorates T2D through dual regulation of hepatic metabolism and gut microbiota (Figure 9). LBTE promoted glycogen synthesis and suppressed lipid accumulation via regulation of key metabolic genes. Furthermore, LBTE reshaped the gut microbiota to enhance SCFA production, which in turn improved intestinal barrier integrity and alleviated hepatic inflammation and metabolic disturbances via the GPR43/GPR109A-mediated signaling pathway. Notably, these beneficial effects were

abrogated upon antibiotic-induced microbiota depletion, confirming a microbiota-dependent mechanism of action. Additionally, quercetin, luteolin, genistein, and kaempferol were identified as the potential active ingredients contributing to the antidiabetic effects of LBTE. Collectively, this study offers new insight into the therapeutic potential of LBTE as a complementary strategy for T2D prevention and management.

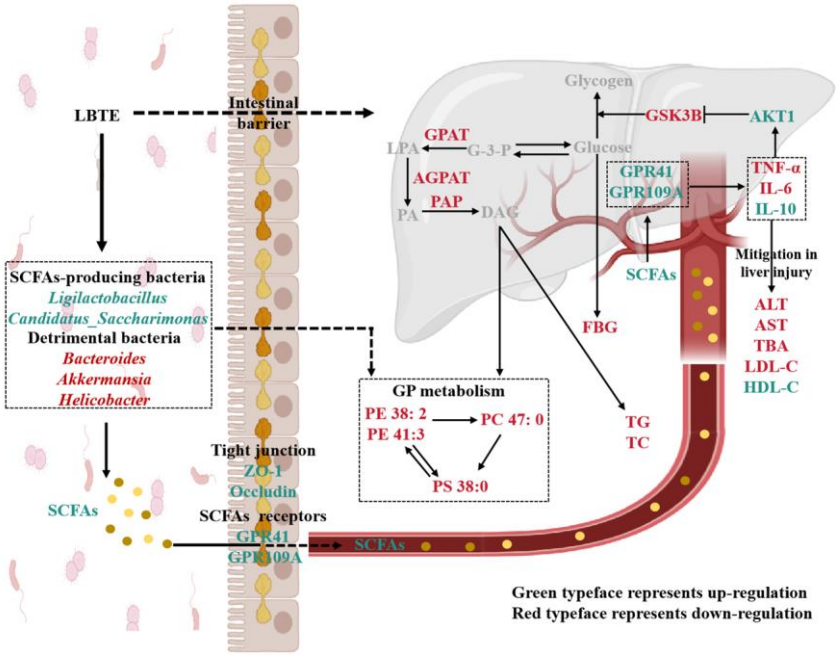


Figure 9. Schematic diagram of LBTE against T2D.

Supplementary Materials: The following supporting information can be downloaded at: https://www.mdpi.com/article/doi/s1, Figure S1: Schematic diagram of the experimental design; Figure S2: Schematic diagram of the experimental design for pseudo-germ-free mouse; Figure S3: Primary chemical constituents of LBTE. LBTE, Liubao tea extract; Figure S4: Total ion chromatogram (TIC) of compounds in LBTE detected by LC-MS; Figure S5: Identification of key active ingredients in LBTE; Figure S6: Molecular docking analysis of the key targets and key core compounds; Figure S7: Effects of different modes of metformin administration on blood glucose in mice; Figure S8: Reproducibility assessment of QC samples in the serum metabolomic analysis; Figure S9: Level distribution of serum differential metabolites shared in the comparison among the four groups; Figure S10: ROC analysis to evaluate the discriminative performance of serum differential metabolites between two groups; Figure S11: Analysis of discriminative gut microbiota and KEGG functional enrichment; Figure S12: Metorigin analysis on gut microbiota and differential metabolites between NC and MC groups; Figure S13: BIO-Sankey Network of gut microbiota and differential metabolites between the NC and MC groups; Figure S14: Metorigin analysis on gut microbiota and differential metabolites between MC and LBTE-L groups; Figure S15: Metorigin analysis on gut microbiota and differential metabolites between MC and LBTE-H groups; Figure S16: Effects of LBTE treatment on the short-chain fatty acids (SCFAs) levels and the intestinal barrier function;Table S1: Chromatographic conditions for chemical composition analysis of LBTE;. Table S2: Mass spectrometric conditions for chemical composition analysis of LBTE; Table S3: Chromatographic conditions for quantitative analysis of potential ingredients in LBTE; Table S4: Mass spectrometric conditions for quantitative analysis of potential ingredients in LBTE; Table S5: Chromatographic conditions for serum metabolomic analysis; Table S6: Mass spectrometric conditions for serum metabolomic analysis; Table S7: Primer sequences for the qPCR analysis; Table S8: Characterization of compounds in LBTE via LC-MS; Table S9: Identification information of the potential bioactive ingredients in LBTE

against T2D; Table S10: Interaction between the key proteins and the potential bioactive compounds from LBTE.

Author Contributions: Conceptualization, J.L. and Q.Z.; methodology, J.L.; software, X.L.; validation, J.L., Y.T. (Yuru Tan), B.Y. and M.W.; formal analysis, J.L.; investigation, J.L. and Z.W.; resources, Q.Z.; data curation, J.L., Y.T. (Ying Tong), X.G., P.Z. and S.X.; writing—original draft preparation, J.L., Z.W.and Y.T. (Yuru Tan); writing—review and editing, J.L., Z.W. and Q.Z.; visualization, J.L.; supervision, Q.Z.; project administration, Q.Z.; funding acquisition, Q.Z. All authors have read and agreed to the published version of the manuscript.

Funding: This work was supported by Natural Science Foundation of Guangxi [No. 2023GXNSFBA026255]; Guangxi Key R&D Program Projects [No. Guike AB25069047 and AB25069175]; National Natural Science Foundation of China [No. 82160804]; Guangxi Zhuang Autonomous Region Administration of Traditional Chinese Medicine (No. GXZYA20240312); Guangxi Science and Technology Major Program [No. Guike AA23073019]; and the Project of Hubei Key Laboratory of Rheumatic Disease Occurrence and Intervention [No. PT022309 and PT022401].

Institutional Review Board Statement: The study was conducted in accordance with the Declaration of Helsinki, and approved by the Animal Experimental Ethics Committee of Guangxi University (No. GXU-2023-0226, 27 December 2023).

Informed Consent Statement: Not applicable.

Data Availability Statement: All data associated with this study are present in the paper. Data are available upon request to the corresponding author.

Conflicts of Interest: The authors declare no conflicts of interest.

References

1. Huang, Z.; Liu, Y.; Liu, X.; Chen, K.; Xiong, W.; Qiu, Y.; He, X.; Liu, B.; Zeng, F. Sanghuangporus vaninii mixture ameliorated type 2 diabetes mellitus and altered intestinal microbiota in mice. Food Funct 2022, 13, 11758-11769.
2. Chen, M.; Pan, P.; Zhang, H.; Li, R.; Ren, D.; Jiang, B. Latilactobacillus sakei QC9 alleviates hyperglycaemia in high-fat diet and streptozotocin-induced type 2 diabetes mellitus mice via the microbiota-gut-liver axis. Food Funct 2024, 15, 8008-8029.
3. Ge, X.; Liu, T.; Chen, Z.; Zhang, J.; Yin, X.; Huang, Z.; Chen, L.; Zhao, C.; Shao, R.; Xu, W. Fagopyrum tataricum ethanol extract ameliorates symptoms of hyperglycemia by regulating gut microbiota in type 2 diabetes mellitus mice. Food Funct 2023, 14, 8487-8503.
4. Luo, Q.; Luo, L.; Zhao, J.; Wang, Y.; Luo, H. Biological potential and mechanisms of Tea's bioactive compounds: An Updated review. J Adv Res 2024, 65, 345-363.
5. Ni, W.J.; Chen, X.X.; Wei, S.Y.; Lan, L.L.; Qiu, R.J.; Ling, Y.P.; Zhou, D.S.; Wu, Z.M.; Cao, Z.H.; Yu, C.P., et al. Study on the mechanism of active components of Liupao tea on 3CL(pro) based on HPLC-DAD fingerprint and molecular docking technique. J Food Biochem 2021, 45, e13707.
6. Cheng, L.; Yang, Q.; Chen, Z.; Zhang, J.; Chen, Q.; Wang, Y.; Wei, X. Distinct Changes of Metabolic Profile and Sensory Quality during Qingzhuan Tea Processing Revealed by LC-MS-Based Metabolomics. J Agric Food Chem 2020, 68, 4955-4965.
7. Qiu, S.; Huang, L.; Xia, N.; Teng, J.; Wei, B.; Lin, X.; Khan, M.R. Two Polysaccharides from Liupao Tea Exert Beneficial Effects in Simulated Digestion and Fermentation Model In Vitro. Foods 2022, 11, 2958.
8. Feng, X.; Chen, M.; Song, H.; Ma, S.; Ou, C.; Li, Z.; Hu, H.; Yang, Y.; Zhou, S.; Pan, Y., et al. A systemic review on Liubao tea: A time-honored dark tea with distinctive raw materials, process techniques, chemical profiles, and biological activities. Compr Rev Food Sci Food Saf 2023, 22, 5063-5085.
9. Wu, Z.; Yu, W.; Ni, W.; Teng, C.; Ye, W.; Yu, C.; Zeng, Y. Improvement of obesity by Liupao tea is through the IRS-1/PI3K/AKT/GLUT4 signaling pathway according to network pharmacology and experimental verification. Phytomedicine 2023, 110, 154633.

10. Yang, S.; Wei, Z.; Luo, J.; Wang, X.; Chen, G.; Guan, X.; She, Z.; Liu, W.; Tong, Y.; Liu, H., et al. Integrated bioinformatics and multiomics reveal Liupao tea extract alleviating NAFLD via regulating hepatic lipid metabolism and gut microbiota. Phytomedicine 2024, 132, 155834.
11. Zhou, H.; Wang, X.; She, Z.; Huang, L.; Wei, H.; Yang, S.; Wei, Z.; Chen, H.; Yang, B.; Hu, Z., et al. Combining bioinformatics and multiomics strategies to investigate the key microbiota and active components of Liupao tea ameliorating hyperlipidemia. J Ethnopharmacol 2024, 333, 118438.
12. Ding, Q.; Zhang, B.; Zheng, W.; Chen, X.; Zhang, J.; Yan, R.; Zhang, T.; Yu, L.; Dong, Y.; Ma, B. Liupao tea extract alleviates diabetes mellitus and modulates gut microbiota in rats induced by streptozotocin and high-fat, high-sugar diet. Biomed Pharmacother 2019, 118, 109262.
13. Zhu, J.; Wu, M.; Zhou, H.; Cheng, L.; Wei, X.; Wang, Y. Liubao brick tea activates the PI3K-Akt signaling pathway to lower blood glucose, metabolic disorders and insulin resistance via altering the intestinal flora. Food Res Int 2021, 148, 110594.
14. Zhao, Y.; Song, P.; Yin, S.; Fan, T.; Li, F.; Ge, X.; Liu, T.; Xu, W.; Xu, S.; Chen, L. Onchidium struma polysaccharides exhibit hypoglycemic activity and modulate the gut microbiota in mice with type 2 diabetes mellitus. Food Funct 2023, 14, 1937-1951.
15. Pabst, O.; Hornef, M.W.; Schaap, F.G.; Cerovic, V.; Clavel, T.; Bruns, T. Gut-liver axis: barriers and functional circuits. Nat Rev Gastroenterol Hepatol 2023, 20, 447-461.
16. Zeng, H.; Liu, C.; Wan, L.; Peng, L.; Wen, S.; Fang, W.; Chen, H.; Wang, K.; Yang, X.; Huang, J., et al. (-)-Epicatechin ameliorates type 2 diabetes mellitus by reshaping the gut microbiota and Gut-Liver axis in GK rats. Food Chem 2024, 447, 138916.
17. Jiang, S.; Liu, A.; Ma, W.; Liu, X.; Luo, P.; Zhan, M.; Zhou, X.; Chen, L.; Zhang, J. Lactobacillus gasseri CKCC1913 mediated modulation of the gut-liver axis alleviated insulin resistance and liver damage induced by type 2 diabetes. Food Funct 2023, 14, 8504-8520.
18. Cui, H.; Hu, D.; Xu, J.; Zhao, S.; Song, Y.; Qin, G.; Liu, Y. Identification of hub genes associated with diabetic cardiomyopathy using integrated bioinformatics analysis. Sci Rep 2024, 14, 15324.
19. Zou, J.; Song, Q.; Shaw, P.C.; Zuo, Z. Dendrobium officinale regulate lipid metabolism in diabetic mouse liver via PPAR-RXR signaling pathway: Evidence from an integrated multi-omics analysis. Biomed Pharmacother 2024, 173, 116395.
20. Hou, F.; Yu, Z.; Cheng, Y.; Liu, Y.; Liang, S.; Zhang, F. Deciphering the pharmacological mechanisms of Scutellaria baicalensis Georgi on oral leukoplakia by combining network pharmacology, molecular docking and experimental evaluations. Phytomedicine 2022, 103, 154195.
21. Hou, Y.; Bai, L.; Wang, X.; Zhang, S.; Liu, S.; Hu, J.; Gao, J.; Guo, S.; Ho, C.T.; Bai, N. Gut Microbiota Combined with Serum Metabolomics to Investigate the Hypoglycemic Effect of Actinidia arguta Leaves. Nutrients 2023, 15, 4115.
22. Liu, X.; Wu, X.; Wang, S.; Zhao, Z.; Jian, C.; Li, M.; Qin, X. Microbiome and metabolome integrally reveal the anti-depression effects of Cistanche deserticola polysaccharides from the perspective of gut homeostasis. Int J Biol Macromol 2023, 245, 125542.
23. Wu, Y.; Sun, H.; Yi, R.; Tan, F.; Zhao, X. Anti-obesity effect of Liupao tea extract by modulating lipid metabolism and oxidative stress in high-fat-diet-induced obese mice. J Food Sci 2021, 86, 215-227.
24. Liao, H.; Zhao, Y.; Liang, Y.; Zou, K. Flavonoids Derived from Opuntia ficus-indica Fruit Alleviate Renal Injury in Diabetic Nephropathy Mice by Altering Gut Microbiota and Promoting the Production of SCFAs. Nutrients 2025, 17.
25. Zhang, Z.; Lai, J.; Fan, X.; Wang, S.; Zhang, H.; Wang, L.; Wang, H. Extraction of polysaccharides from Polygonum cuspidatum with activity against Type 2 Diabetes via alterations in gut microbiota. Food Chem 2025, 470, 140047.
26. Chen, Y.; Zhu, L.; Hu, W.; Wang, Y.; Wen, X.; Yang, J. Simiao Wan modulates the gut microbiota and bile acid metabolism during improving type 2 diabetes mellitus in mice. Phytomedicine 2022, 104, 154264.
27. Qian, Y.; Zhang, J.; Fu, X.; Yi, R.; Sun, P.; Zou, M.; Long, X.; Zhao, X. Preventive Effect of Raw Liubao Tea Polyphenols on Mouse Gastric Injuries Induced by HCl/Ethanol via Anti-Oxidative Stress. Molecules 2018, 23.
28. Chen, G.; Xie, M.; Wan, P.; Chen, D.; Dai, Z.; Ye, H.; Hu, B.; Zeng, X.; Liu, Z. Fuzhuan Brick Tea Polysaccharides Attenuate Metabolic Syndrome in High-Fat Diet Induced Mice in Association with Modulation in the Gut Microbiota. J Agric Food Chem 2018, 66, 2783-2795.

29. Yan, G.; Qin, Z.; Liu, A.; Huang, Z.; Wang, X.; Zhang, S.; Xie, X.; Huang, X.; Chen, J.; Li, Y., et al. Sulfonation metabolism in the gut microbiota is the main metabolic pathway of cholesterol in hypercholesterolemic mice. Food Funct 2024, 15, 9750-9765.
30. Yuan, X.; Wang, R.; Han, B.; Sun, C.; Chen, R.; Wei, H.; Chen, L.; Du, H.; Li, G.; Yang, Y., et al. Functional and metabolic alterations of gut microbiota in children with new-onset type 1 diabetes. Nat Commun 2022, 13, 6356.
31. Yu, G.; Xu, C.; Zhang, D.; Ju, F.; Ni, Y. MetOrigin: Discriminating the origins of microbial metabolites for integrative analysis of the gut microbiome and metabolome. Imeta 2022, 1, e10.
32. Zhang, S.; Wang, H.; Zhu, M.J. A sensitive GC/MS detection method for analyzing microbial metabolites short chain fatty acids in fecal and serum samples. Talanta 2019, 196, 249-254.
33. Graham, G.G.; Punt, J.; Arora, M.; Day, R.O.; Doogue, M.P.; Duong, J.K.; Furlong, T.J.; Greenfield, J.R.; Greenup, L.C.; Kirkpatrick, C.M., et al. Clinical pharmacokinetics of metformin. Clin Pharmacokinet 2011, 50, 81-98.
34. Wang, Z.; Zeng, M.; Wang, Z.; Qin, F.; Chen, J.; He, Z. Dietary Luteolin: A Narrative Review Focusing on Its Pharmacokinetic Properties and Effects on Glycolipid Metabolism. J Agric Food Chem 2021, 69, 1441-1454.
35. Yan, L.; Vaghari-Tabari, M.; Malakoti, F.; Moein, S.; Qujeq, D.; Yousefi, B.; Asemi, Z. Quercetin: an effective polyphenol in alleviating diabetes and diabetic complications. Crit Rev Food Sci Nutr 2023, 63, 9163-9186.
36. Yao, Y.X.; Yu, Y.J.; Dai, S.; Zhang, C.Y.; Xue, X.Y.; Zhou, M.L.; Yao, C.H.; Li, Y.X. Kaempferol efficacy in metabolic diseases: Molecular mechanisms of action in diabetes mellitus, obesity, non-alcoholic fatty liver disease, steatohepatitis, and atherosclerosis. Biomed Pharmacother 2024, 175, 116694.
37. Bai, Z.; Huang, X.; Wu, G.; Zhou, Y.; Deng, X.; Yang, J.; Yin, J.; Nie, S. Hepatic metabolism-related effects of polysaccharides from red kidney bean and small black soybean on type 2 diabetes. Food Chem 2023, 403, 134334.
38. Liu, H.; Guo, X.; Jiang, K.; Shi, B.; Liu, L.; Hou, R.; Chen, G.; Farag, M.A.; Yan, N.; Liu, L. Dietary polyphenols regulate appetite mechanism via gut-brain axis and gut homeostasis. Food Chem 2024, 446, 138739.
39. Panickar, K.S. Effects of dietary polyphenols on neuroregulatory factors and pathways that mediate food intake and energy regulation in obesity. Mol Nutr Food Res 2013, 57, 34-47.
40. Blachnio-Zabielska, A.; Hajduch, E.; Le Stunff, H. Editorial: The Role of Sphingolipid Metabolism in the Development of Type 2 Diabetes and Obesity. Front Endocrinol (Lausanne) 2021, 12, 835751.
41. Chen, L.; Wang, J.; Ren, Y.; Ma, Y.; Liu, J.; Jiang, H.; Liu, C. Artesunate improves glucose and lipid metabolism in db/db mice by regulating the metabolic profile and the MAPK/PI3K/Akt signalling pathway. Phytomedicine 2024, 126, 155382.
42. Yang, X.; Liu, Y.; Tang, Z.; Song, Z.; Liu, C.; Wang, C. Total flavonoids of Hippophae rhamnoides L. improves type 2 diabetes symptoms in rats through down-regulating of the DAG/PRKCA/MAPK10/p65/TNF-α signalling pathway. J Ethnopharmacol 2024, 318, 116962.
43. Di Sarli Gutiérrez, L.; Castro, M.C.; Farromeque Vásquez, S.; Villagarcía, H.G.; González Arbeláez, L.; Rojano, B.; Schinella, G.; Maiztegui, B.; Francini, F. Protective Effect of Monoterpene Isoespintanol in a Rat Model of Prediabetes Induced by Fructose. Pharmaceuticals (Basel) 2023, 17, 47.
44. Comba, S.; Menendez-Bravo, S.; Arabolaza, A.; Gramajo, H. Identification and physiological characterization of phosphatidic acid phosphatase enzymes involved in triacylglycerol biosynthesis in Streptomyces coelicolor. Microb Cell Fact 2013, 12, 9.
45. Song, Q.; Zhang, K.; Li, S.; Weng, S. Trichosanthes kirilowii Maxim. Polysaccharide attenuates diabetes through the synergistic impact of lipid metabolism and modulating gut microbiota. Curr Res Food Sci 2025, 10, 100977.
46. Wang, F.; Xu, S.J.; Ye, F.; Zhang, B.; Sun, X.B. Integration of Transcriptomics and Lipidomics Profiling to Reveal the Therapeutic Mechanism Underlying Ramulus mori (Sangzhi) Alkaloids for the Treatment of Liver Lipid Metabolic Disturbance in High-Fat-Diet/Streptozotocin-Induced Diabetic Mice. Nutrients 2023, 15, 3914.
47. Song, H.; Xue, H.; Zhang, Z.; Wang, J.; Li, A.; Zhang, J.; Luo, P.; Zhan, M.; Zhou, X.; Chen, L., et al. Amelioration of Type 2 Diabetes Using Four Strains of Lactobacillus Probiotics: Effects on Gut Microbiota Reconstitution-Mediated Regulation of Glucose Homeostasis, Inflammation, and Oxidative Stress in Mice. J Agric Food Chem 2023, 71, 20801-20814.

48. Huang, H.; Chen, J.; Hu, X.; Chen, Y.; Xie, J.; Ao, T.; Wang, H.; Xie, J.; Yu, Q. Elucidation of the interaction effect between dietary fiber and bound polyphenol components on the anti-hyperglycemic activity of tea residue dietary fiber. Food Funct 2022, 13, 2710-2728.
49. Qin, J.; Li, Y.; Cai, Z.; Li, S.; Zhu, J.; Zhang, F.; Liang, S.; Zhang, W.; Guan, Y.; Shen, D., et al. A metagenome-wide association study of gut microbiota in type 2 diabetes. Nature 2012, 490, 55-60.
50. Ye, J.; Ma, J.; Rozi, P.; Kong, L.; Zhou, J.; Luo, Y.; Yang, H. The polysaccharides from seeds of Glycyrrhiza uralensis ameliorate metabolic disorders and restructure gut microbiota in type 2 diabetic mice. Int J Biol Macromol 2024, 264, 130622.
51. Dogan, Z.; Sarikaya, M.; Ergul, B.; Filik, L. The effect of Helicobacter pylori eradication on insulin resistance and HbA1c level in people with normal glucose levels: a prospective study. Biomed Pap Med Fac Univ Palacky Olomouc Czech Repub 2015, 159, 242-245.
52. Ma, Z.; Sun, W.; Wang, L.; Wang, Y.; Pan, B.; Su, X.; Li, H.; Zhang, H.; Lv, S.; Wang, H. Integrated 16S rRNA sequencing and nontargeted metabolomics analysis to reveal the mechanisms of Yu-Ye Tang on type 2 diabetes mellitus rats. Front Endocrinol (Lausanne) 2023, 14, 1159707.
53. Su, M.; Hu, R.; Tang, T.; Tang, W.; Huang, C. Review of the correlation between Chinese medicine and intestinal microbiota on the efficacy of diabetes mellitus. Front Endocrinol (Lausanne) 2022, 13, 1085092.
54. Manilla, V.; Santopaolo, F.; Gasbarrini, A.; Ponziani, F.R. Type 2 Diabetes Mellitus and Liver Disease: Across the Gut-Liver Axis from Fibrosis to Cancer. Nutrients 2023, 15, 2521.
55. Zhang, Y.; Wang, J.; Ge, W.; Song, Y.; He, R.; Wang, Z.; Zhao, L. Camel milk peptides alleviate hyperglycemia by regulating gut microbiota and metabolites in type 2 diabetic mice. Food Res Int 2023, 173, 113278.
56. Zuo, Z.; Pang, W.; Sun, W.; Lu, B.; Zou, L.; Zhang, D.; Wang, Y. Metallothionein-Kidney Bean Polyphenol Complexes Showed Antidiabetic Activity in Type 2 Diabetic Rats by Improving Insulin Resistance and Regulating Gut Microbiota. Foods 2023, 12, 3139.
57. Min, Q.; Wang, Y.; Jin, T.; Zhu, L.; Wu, X.; Li, Y.; Wang, Y.; Xu, N. Analysis of Intestinal Short-Chain Fatty Acid Metabolism Profile After Probiotics and GLP-1 Treatment for Type 2 Diabetes Mellitus. Front Endocrinol (Lausanne) 2022, 13, 892127.
58. Saad, M.J.; Santos, A.; Prada, P.O. Linking Gut Microbiota and Inflammation to Obesity and Insulin Resistance. Physiology (Bethesda) 2016, 31, 283-293.
59. Wen, X.; Xiaoyue, D.; Longkun, D.; Yue, X.; Man, Y.; Min, Z.; Liang, W.; Chengxue, Y.; Huaxi, X. Three main short-chain fatty acids inhibit the activation of THP-1 cells by Mycoplasma pneumoniae. Biosci Biotechnol Biochem 2021, 85, 923-930.
60. Guo, Q.; Wang, X.; Ke, J.; Hou, X.; Shen, G.; Li, S.; Chen, H.; Cui, Q.; Yu, J.; Luo, Q., et al. Chayote pectin regulates blood glucose through the gut-liver axis: Gut microbes/SCFAs/FoxO1 signaling pathways. Food Res Int 2025, 202, 115706.
61. Gao, Z.; Dai, H.; Zhang, Q.; Yang, F.; Bu, C.; Chen, S. Hydroxytyrosol Alleviates Acute Liver Injury by Inhibiting the TNF-α/PI3K/AKT Signaling Pathway via Targeting TNF-α Signaling. Int J Mol Sci 2024, 25, 12844.
62. Mueller, N.T.; Zhang, M.; Juraschek, S.P.; Miller, E.R.; Appel, L.J. Effects of high-fiber diets enriched with carbohydrate, protein, or unsaturated fat on circulating short chain fatty acids: results from the OmniHeart randomized trial. Am J Clin Nutr 2020, 111, 545-554.